To the Graduate Council:

I am submitting herewith a thesis written by Kenneth A. Lienemann entitled "Calibration of a Germanium Bolometer for Use in Cold-Background Radiometric Testing." I have examined the final copy of this thesis for form and content and recommend that it be accepted in partial fulfillment of the requirements for the degree of Master of Science, with a major in Engineering Science.

Firouz Shahrokhi, Major Professor

We have read this thesis
and recommend its acceptance:

C. J. N. Paludan

Frank D. Collins

Accepted for the Council:

The Graduate School

STATEMENT OF PERMISSION TO USE

In presenting this thesis in partial fulfillment of the requirements for a Master's degree at The University of Tennessee, Knoxville, I agree that the Library shall make it available to borrowers under rules of the Library. Brief quotations from this thesis are allowable without special permission, provided that accurate acknowledgment of the source is made.

Permission for extensive quotation from or reproduction of this thesis may be granted by my major professor, or in his absence, by Head of Interlibrary Services when, in the opinion of either, the proposed use of the material is for scholarly purposes. Any copying or use of the material in this thesis for financial gain shall not be allowed without my written permission.

Signature Kenneth A. Liemann

Date May 13, 1985

CALIBRATION OF A GERMANIUM BOLOMETER FOR USE IN COLD-BACKGROUND RADIOMETRIC TESTING

A Thesis

Presented for the

Master of Science

Degree

The University of Tennessee, Knoxville

Kenneth A. Lienemann

June 1985

ACKNOWLEDGMENTS

The author would like to express his gratitude to Calspan Corporation and Arnold Engineering Development Center (AEDC). The work reported herein was sponsored by Headquarters, AEDC, Air Force Systems Command (AFSC), under Program Element No. 65807F, Contract No. F40600-81C-0003. The results reported herein were obtained by Calspan Corporation, a contract operator at AEDC, AFSC, Arnold Air Force Station, Tennessee, under AEDC Project No. CA13VS. Further reproduction of this document is authorized to satisfy the needs of the U.S. Government.

Many people, too numerous to mention, have contributed to the development of infrared expertise at AEDC, and their efforts are tacitly recognized here. Much credit is due to Messrs. Jay Hiatt and Herb Little for guidance on calibration philosophy. Special thanks to Ms. Cheryl Williams for her help in preparing the figures. Cheryl is one of those unrecognized "little" people, without whom nothing would ever get done.

Finally, the author would like to express his appreciation to Dr. Firouz Shahrokhi, Dr. Ted Paludan, and Dr. Frank Collins, who served as director and members of the thesis committee. They provided criticism and encouragement; however, any errors or omissions are the responsibility of the author.

ABSTRACT

A germanium bolometer has been obtained and evaluated for possible use in radiometric testing. The instrument and test procedures are described, and results are presented which detail the bolometer's response to a variety of operating conditions. Suggested improvements to the bolometer and the test procedure are given for future work. It is concluded that the bolometer is highly repeatable and will be a useful tool in the transfer of radometric calibration.

TABLE OF CONTENTS

CHAPTER		PAGE
I.	INTRODUCTION.	1
II.	APPARATUS	4
	Bolometer	4
	Physical.	4
	Amplification and electrical.	7
	Cryogenic system.	9
	Test Apparatus.	9
	Filling the helium dewar.	11
	Pumping the helium dewar.	14
	Bench test configuration.	16
	Chamber calibration	16
	Instrumentation	18
	Data Acquisition/Processing	22
III.	TEST DESCRIPTION.	25
	Bench Check	25
	Noise	28
	Load Curve.	29
	Frequency Response.	33
	Chamber Calibration	35
IV.	RESULTS	39
	Data Reduction and Corrections.	39
	Discussion of Results	58
V.	UNCERTAINTY	65

CHAPTER PAGE

VI. FUTURE WORK 72

VII. CONCLUSIONS 76

BIBLIOGRAPHY. 77

APPENDIXES. 80

A. NOISE MEASUREMENTS. 81

B. DIMENSIONAL PARAMETERS AND CORRECTIONS. 95

C. UNCERTAINTY 106

VITA. 116

LIST OF TABLES

TABLE		PAGE
1.	Bolometer Data.	40
2.	Corrected Results	49
3.	Dynamic Data Obtained on March 13, 1984 (50 points/sample).	59
4.	Experimental Uncertainty.	66
5.	Data Uncertainty.	68
6.	Data Acquisition Scheme	75
A-1.	Amplifier Specifications.	83
B-1.	Bolometer Internal Measurements	97
B-2.	Helium Vapor Pressure/Temperature	104
C-1.	Fluke 2204A Voltmeter Calibration (I-66727)	108
C-2.	EG&G 5206 Lock-In Calibration (I-66950)	110
C-3.	Potential Voltage Error	112
C-4.	Derivation of Experimental Uncertainty.	115

LIST OF FIGURES

FIGURE		PAGE
1.	Operating Calibration Ranges (300K, 0.243 mrad source) for 7V Chamber	2
2.	Bolometer Optical Layout	5
3.	Bolometer Mount Layout	6
4.	Bolometer/Amplifier Circuitry	8
5.	Bolometer Cryogenic and Vacuum Systems	10
6.	Bolometer Pumping System	12
7.	Helium Liquid/Vapor Separator	13
8.	Bench Test Schematic	17
9.	Chamber Calibration Schematic	19
10.	Bolometer Calibration Installation	20
11.	Chamber Instrumentation Schematic	21
12.	Bolometer Calibration Data Feeds	23
13.	Bolometer Response to Operating Temperature	27
14.	Typical Load Curve	31
15.	Bolometer Load Curves	32
16.	Bolometer Frequency Response	34
17.	Chopper Tare Correction	37
18.	Internal Calibrator Response to Small Fluctuations in Dewar Pressure	43
19.	Data Sample Diagnostic Plots	47

FIGURE PAGE

20. Bolometer Calibration Results, Data Obtained by Standard Method 52
21. Dynamic Data, 50 Points per Sample 57
22. Dynamic Responsivity 60
23. Inclusive Bolometer Responsivity Results . . . 61
24. Responsivity Curve Fit and Scatter 62
A- 1. Bolometer/Amplifier Simplified Circuit 82
A- 2. Bolometer Noise Spectrum 85
A- 3. Bolometer Diagnostic Circuit 89
A- 4. Zero Bias Noise Spectrum 90
A- 5. Normal Bias Noise Spectrum 90
A- 6. Noise Spectrum with Chopper Harmonics. 91
A- 7. Noise Spectrum: Communications Surge 91
A- 8. Noise Spectrum: Comparison with/without Tektronix® Active. 92
B- 1. Bolometer Internal Measurements Points 96
B- 2. Bolometer-Source Fixture Separation. 99
B- 3. Spectral Absorptivity of Nextel® Black Velvet Paint 101

CHAPTER I

INTRODUCTION

The calibration and testing of long wavelength infrared (LWIR) sensors have been conducted at Arnold Engineering Development Center (AEDC) since 1968. The extremely low irradiance levels required make the generation and calibration of the sources a difficult problem. In 1980 an AEDC standard infrared source (SIRS) was calibrated against an absolute standard by the National Bureau of Standards (NBS), making possible an absolute accuracy assessment for all AEDC infrared source measurements [1].[1] The SIRS is a blackbody cavity, and its output is up to 10 orders of magnitude higher than is required for sensor testing. Figure 1 illustrates the range of radiant intensities (irradiance) covered by the AEDC sources. The transfer of the SIRS calibration to other sources is accomplished through a series of steps [2] which begin with use of a transfer standard detector, a silicon bolometer [1,3,4,5]. This bolometer and its helium dewar are built into a small vacuum chamber which will accommodate a single source for testing. Thus, the transfer to any working source involves a second chamber installation,

---

[1]Numbers in brackets refer to similarly numbered references in the Bibliography.

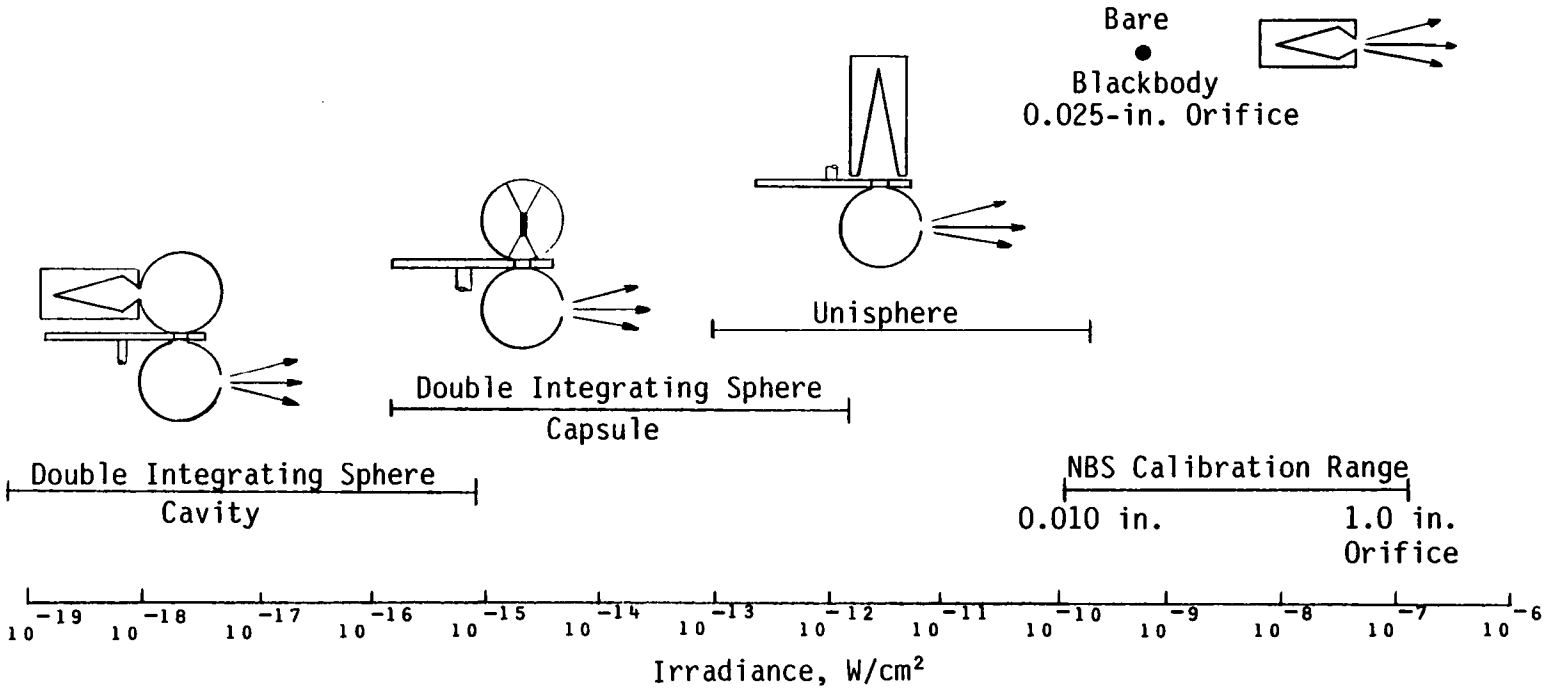


Figure 1. Operating Calibration Ranges (300K, 0.243 mrad source) for 7V Chamber.

resulting in a bias error which increases the total uncertainty of measurement. The chain of calibration transfers through the range of attenuated sources is discussed in Ref. [6].

The initial bias error can be eliminated if the transfer is accomplished in a chamber large enough to accommodate more than one infrared source. In preparation for such a process, a new bolometer has been purchased. This study describes the bolometer, its operating characteristics, and the results of tests to determine its suitability as a transfer standard.

CHAPTER II

APPARATUS

A. Bolometer

A.1 Physical

A bolometer is a thermal detector with a strong negative temperature coefficient of resistance. As the bolometer element is cooled to an operating temperature of 2K, its resistance increases into the megohm (MΩ) range. Infrared (IR) radiation, when absorbed by the bolometer, will change its temperature very slightly, but will result in significant variation in the resistance. Under these conditions, a constant bias on the detector yields a voltage change which is amplified into a signal.

The active bolometer element is a germanium chip suspended within a small gold-coated cavity. The element is heavily overcoated on both faces with 3M Nextel® Black Velvet paint to ensure uniform spectral response [7]. Figure 2 illustrates the optical layout. The path contains cold field stops and apertures which limit the bolometer field of view to 3.9 deg (0.0225 sr). Details of the bolometer element mount are shown in Fig. 3. A small aperture in the rear of the cavity admits energy from the internal calibrator source, a Motorola MLED-910® GaAs emitter mounted behind a 1-mm aperture. This source is

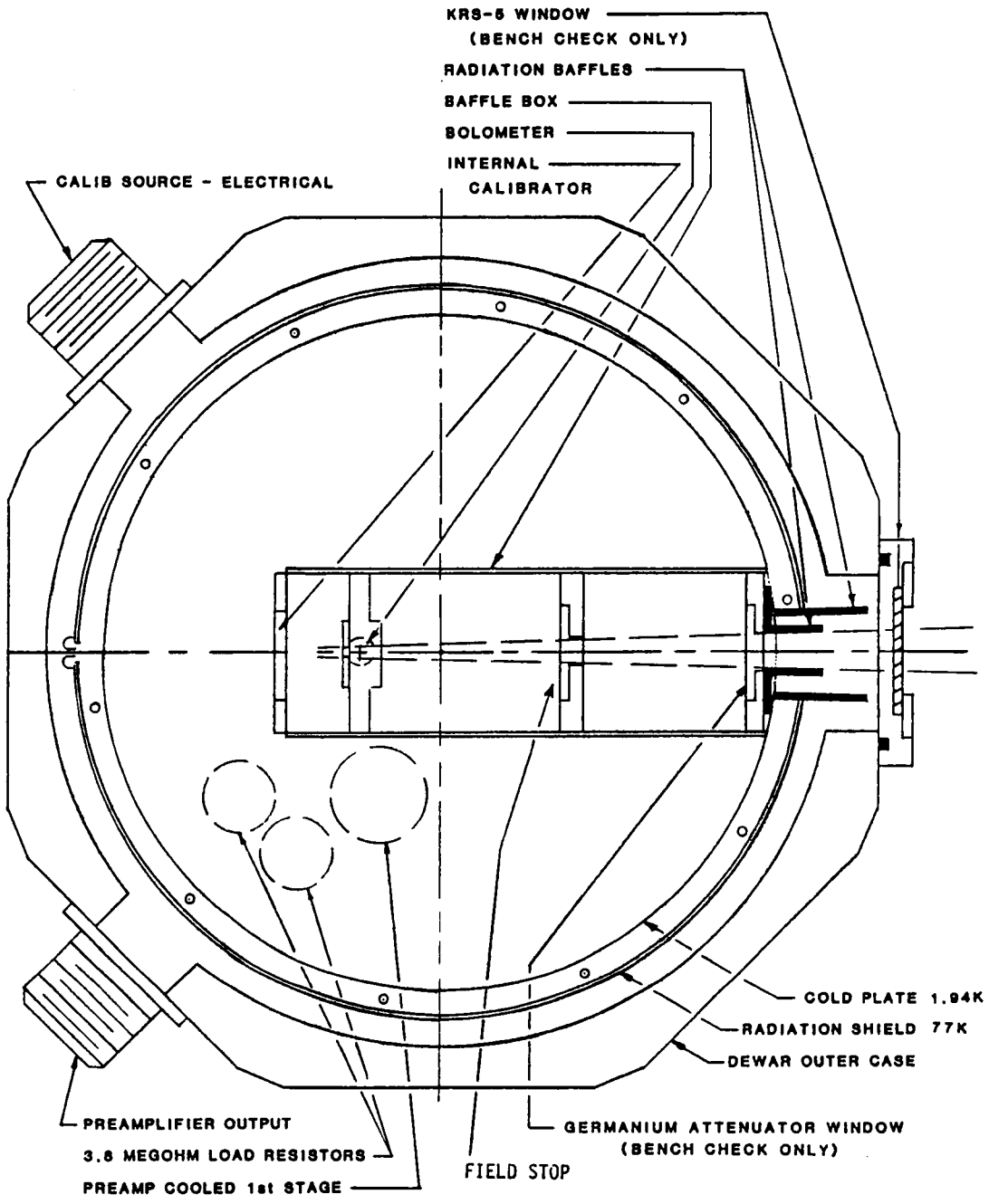


Figure 2. Bolometer Optical Layout.

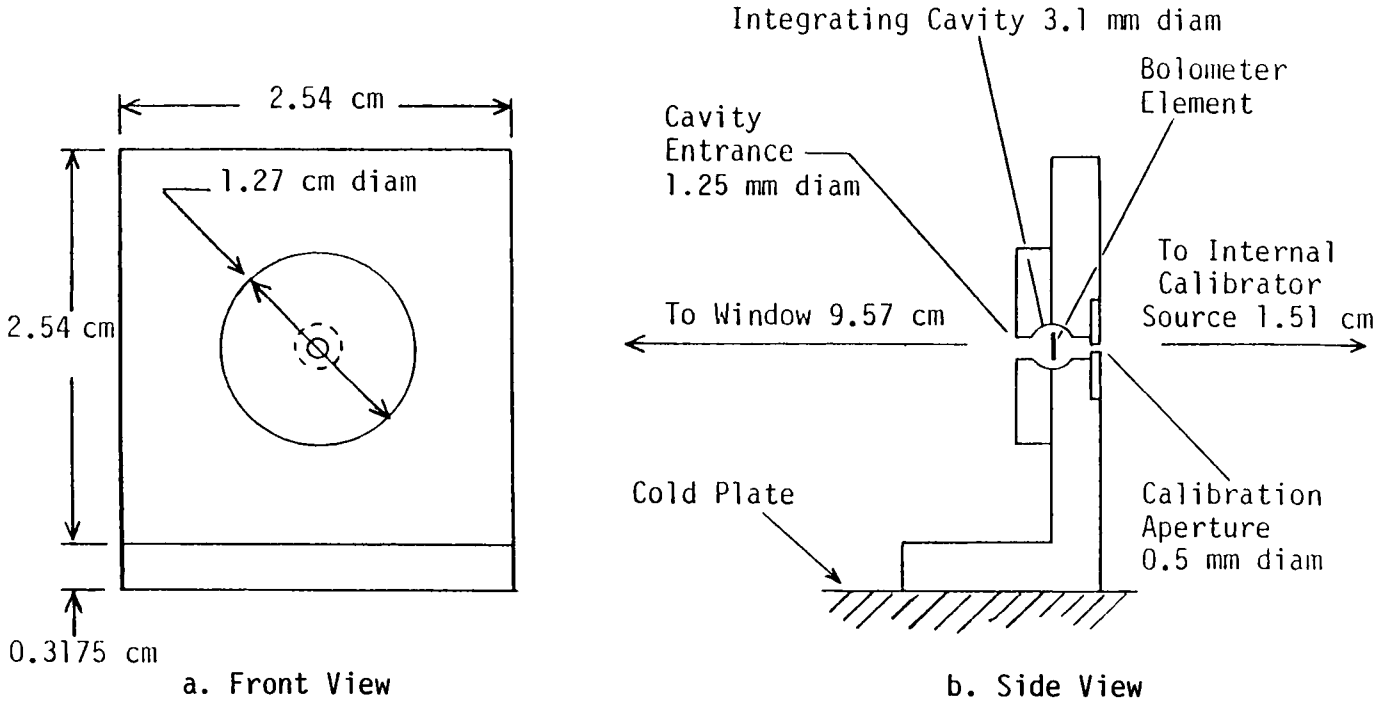


Figure 3. Bolometer Mount Layout.

driven from a regulated square wave oscillator with a frequency of 7.8 Hz.

A.2 Amplification and Electrical

Bolometer signals are subject to two phases of amplification. Impedance matching of the bolometer element and the external amplifier is performed inside the vacuum housing by a field effect transistor (FET). This device cannot operate at liquid helium (LHe) temperatures and is therefore mounted on a standoff away from the cold plate and is provided with a small heater resistor (Fig. 4). The gain provided by the FET is essentially equal to one. The main (external) amplifier is also shown in Fig. 4. The signal is first A.C.-coupled and then passed through two op-amps for a total gain of 910.

The bolometer was designed to operate on 9V battery power to eliminate 60-cycle noise and to make it fully portable by avoiding bulky power supplies. Bolometer bias and amplifier bias are separate circuits. Battery drain in the amplifier circuit proved to be excessive and caused significant variation in the data. This effect was recorded during the bench check, and the batteries were then replaced by Lambda LQ-521® power supplies for the duration of calibration.

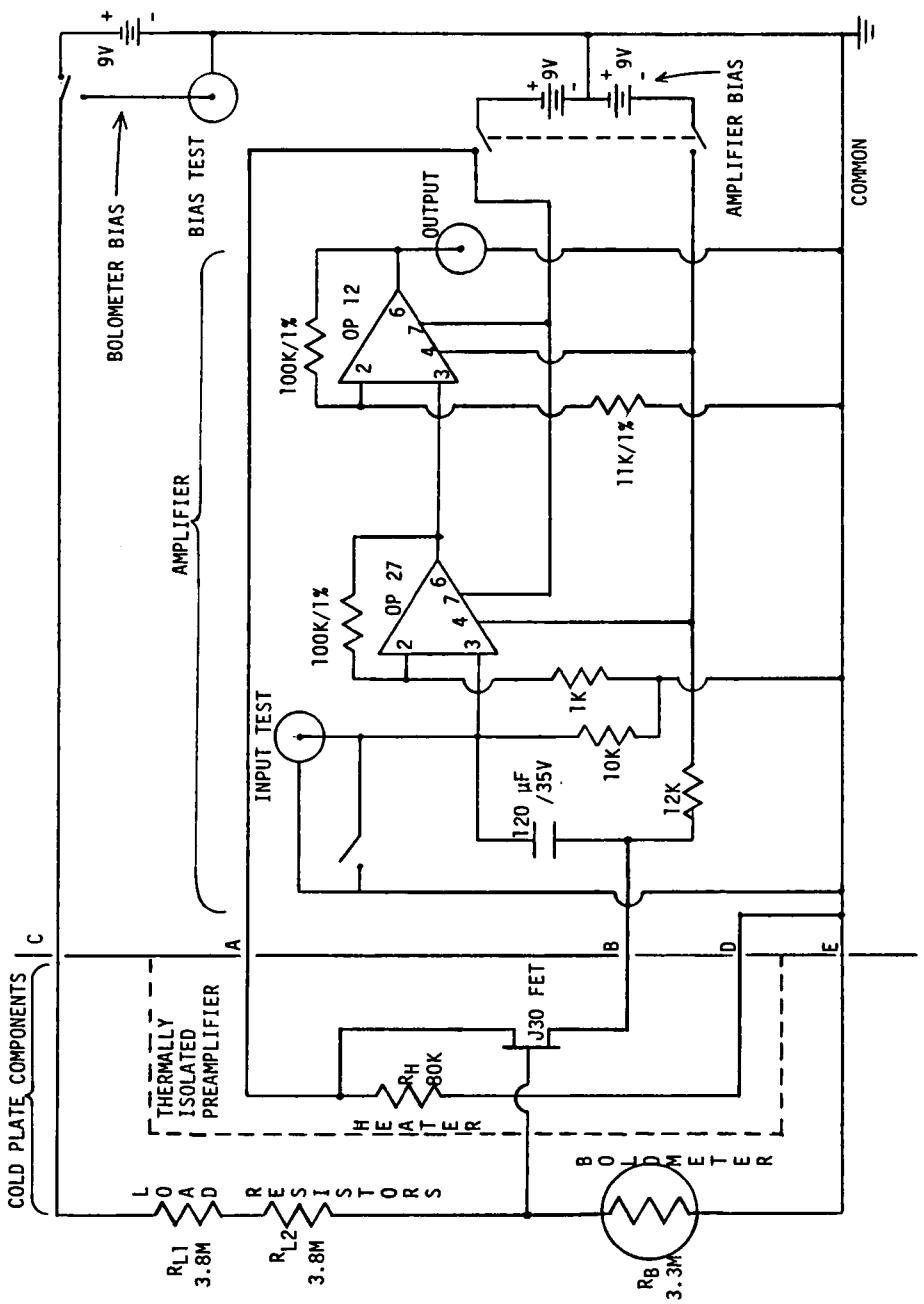


Figure 4. Bolometer/Amplifier Circuitry.

A.3 Cryogenic System

As mentioned earlier, the sensitivity of the bolometer is dependent upon cold temperatures to achieve high resistance. Bolometer cryogenic conditions are maintained by a vacuum jacket, a liquid nitrogen (LN_2) dewar and cold shield at 77K, and a central liquid helium dewar (T less than 4.2K). Figure 5 shows a cross section of the bolometer housing and cryogenic systems. A cold finger on the bottom of the LHe dewar contains the active germanium element (Fig. 3). Room temperature resistance of the bolometer is 30 Ω. Liquid helium temperature (4.2K) increases this to 150ΩK ; however, the sensitivity is still too low for radiation levels used in sensor testing. By pumping the vapor boiling off of the LHe surface, the bath can be supercooled to 1.95K. This temperature corresponds to 20-mm vapor pressure and increases the resistance to 3.3 MΩ.

B. Test Apparatus

Testing and calibration of the bolometer was performed in three phases. First was the bolometer function check on the laboratory bench; then came radiometric calibration in the Component Checkout Chamber (C^3). The final phase was again on the bench and involved resolution of performance parameters and acquisition of some high background calibration points. The same measurements were

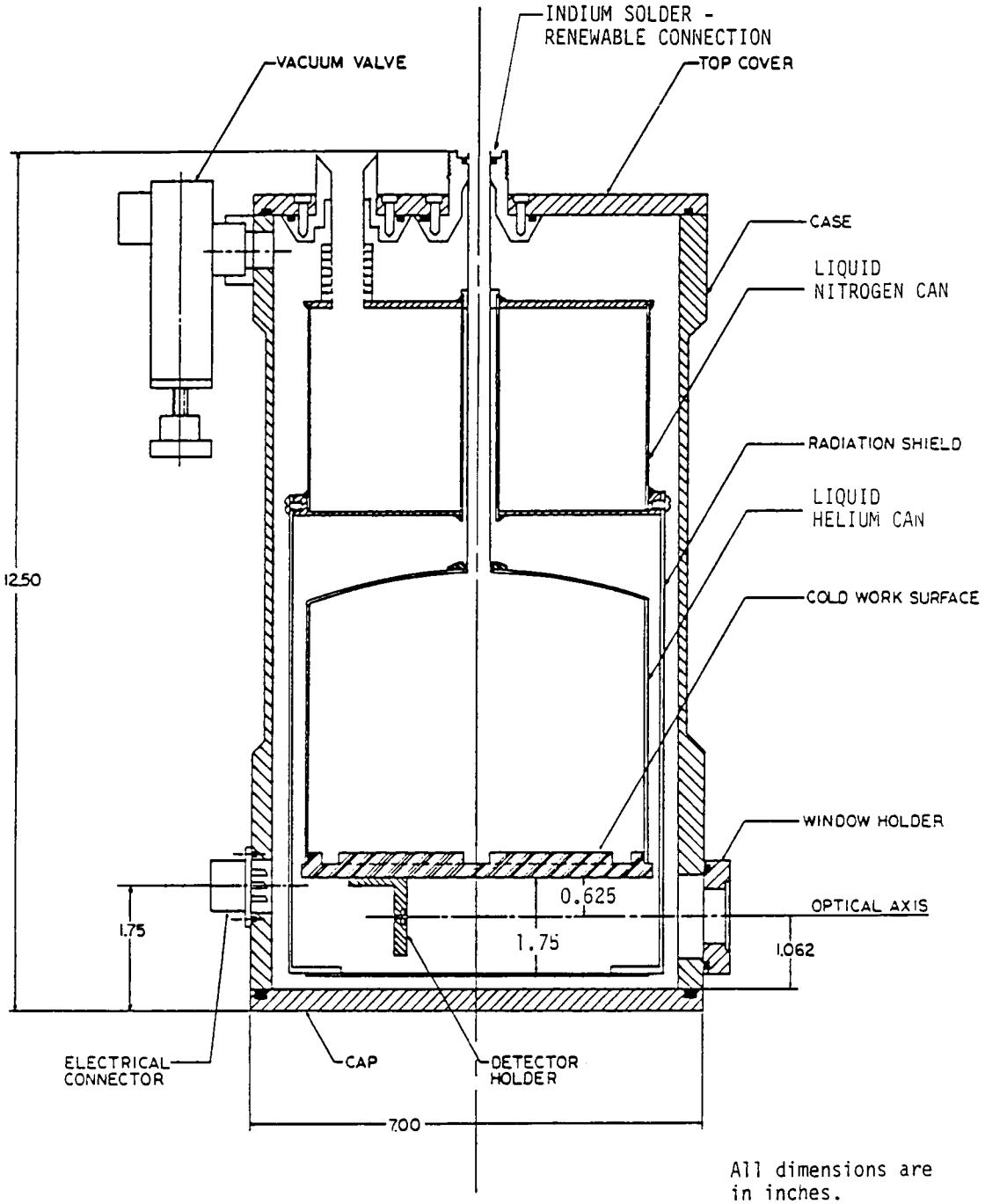


Figure 5. Bolometer Cryogenic and Vacuum Systems.

made in either environment; however, there were procedural variations; the bolometer configuration was changed, and some pieces of test hardware were exchanged for their cryogenic/ambient counterpart.

B.1 Filling the Helium Dewar

B.1.a Bench check. Both dewars are precooled with LN_2 for bench testing of the bolometer. After cold soaking for 30 minutes, the dewars are emptied by inverting the unit, and then each is refilled with the appropriate cryogen. Liquid helium is forced from a storage dewar with 2 psi positive pressure through a vacuum-jacketed transfer line. A full helium dewar is inferred by observing plume characteristics and elapsed time and confirmed by using a balance beam scale to measure the mass increase.

B.1.b Chamber calibration. Cooling the bolometer in the chamber involves a number of significant variations. The LN_2 dewar is cooled conductively by thermal linkage to the 20K chamber cold plate; this places a lower heat load on the helium dewar, and greatly simplifies chamber plumbing. Figure 6 is a schematic of the helium cryogen system. Fill and pumping lines penetrate the chamber through a flange in the base and meet in a liquid/vapor separator on the top of the bolometer (Fig. 7). Liquid passes into the bolometer dewar while vapor exits through

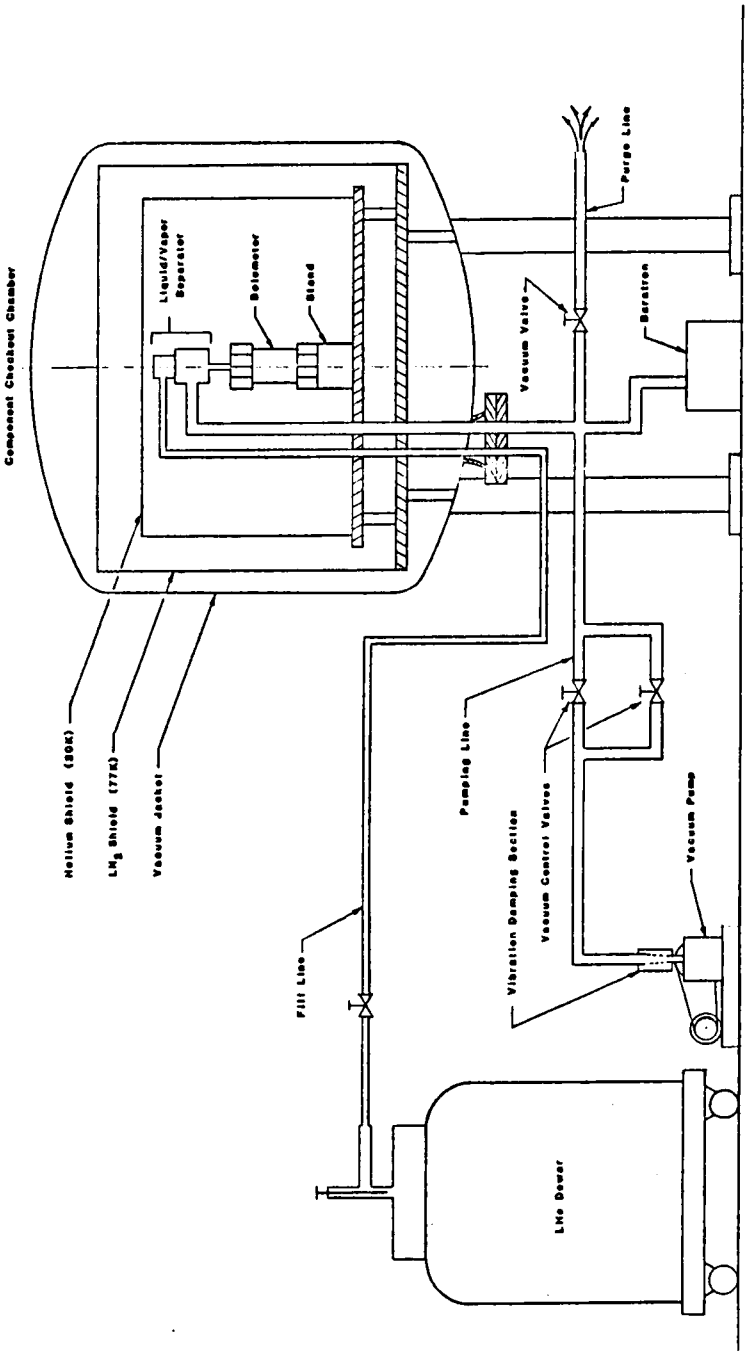


Figure 6. Bolometer Pumping System.

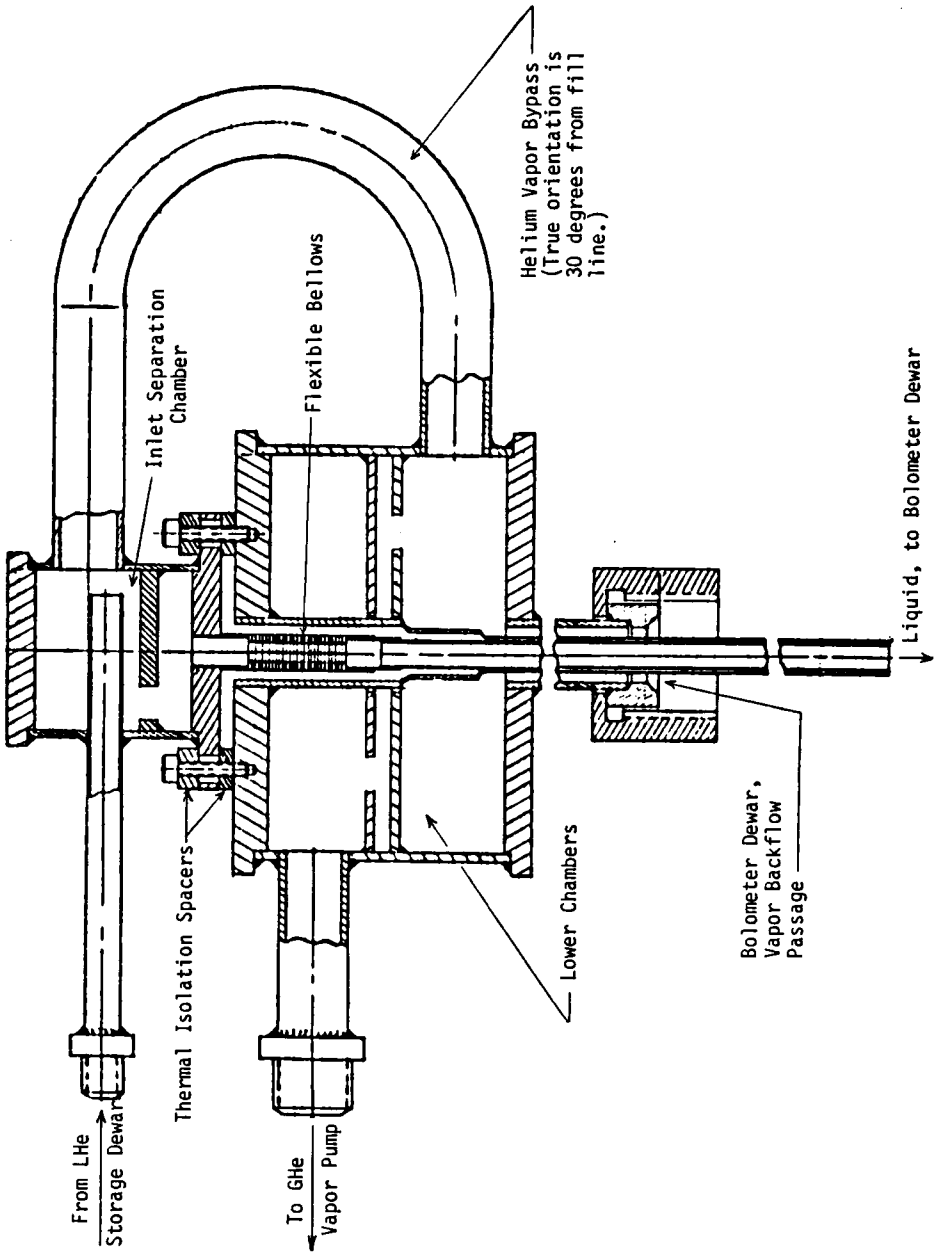


Figure 7. Helium Liquid/Vapor Separator.

the pumping line. Initially, all helium entering the dewar will flash to vapor and leave via the pumping line, but as the bolometer mass cools, liquid begins to accumulate. When the dewar is completely full, LHe overflows the liquid vapor separator and out the pumping line (Fig. 6). During the fill process, the pump is valved off and helium vapor is vented through the purge line. Plume changes (and temperature sensor readings) indicate when the LHe dewar is full. Filling the dewar generally takes 10 minutes and consumes between 5 and 15 liters of LHe.

B.2 Pumping the Helium Dewar

When the bolometer dewar is full, flow from the storage dewar is shut off, the purge line is valved off, and the pumping valve is opened to begin supercooling. Pumping procedures are the same whether the bolometer is on the bench or in the chamber. The objective is to get the bolometer to a stable operating point without consuming too much time or liquid helium. Twenty millimeters (1.94K) can be reached in 60 to 90 minutes, but problems may arise during the process.

Sudden surges in dewar pressure indicate that energy in the form of acoustic waves is being transmitted to the bolometer. This phenomenon is a function of the frequency and magnitude of pump vibration and the length, diameter, materials, and configuration of the pumping

lines. Reference [8] discusses this problem and its solutions in some detail.

Initial attempts to pump the dewar were through a flat-bottom vacuum valve; however, the bolometer was found to have great sensitivity to small pressure variation and the flat valve provided insufficient control. A Manostat® regulator was tried, but while it provided fine control, the constriction was so great that several hours were required to reach test conditions. Numerous iterations of line length and size and the insertion of a ballast chamber in the pumping line were attempted to reduce acoustical transmission.

The final solution depicted in Fig. 6 utilized a Sergent-Welch® 1402 vacuum pump, 6 ft of 1/2-in. tubing and 5-1/2 ft of 1/4-in. tubing. Two needle valves in parallel provided fine pressure resolution and proper pumping speed. Additional pumping line constrictions included the liquid/vapor separator and four 90-deg bends. Connection to the pump was made with 12 in. of neoprene hose to dampen motor vibration.

During bench testing, a heavy coating of frost and ice would occasionally form on the pumping line. This buildup was symptomatic of high mass flow rate through the line and was sometimes attributable to the acoustical phenomenon discussed above. In other instances a poor

insulating vacuum or some other problem was causing the helium to boil very rapidly.

B.3 Bench Test Configuration

For bench testing, the bolometer housing was evacuated and both dewars were filled with the appropriate cryogen. A KRS-5 window (25.4-mm-diam x 2-mm-thick) and a cold germanium window (11-mm-diam x 1-mm-thick) attenuated radiation to prevent detector saturation and signal overload. The transmission of these windows was 68.5 and 41 percent, respectively. The outer KRS-5 window also served the purpose of completing the vacuum integrity of the bolometer housing. The radiation source was a Barnes® 11-200T calibrated blackbody cavity with a 5.232-mm-diam output aperture. The initial checkout utilized a two-blade, 50-percent-duty chopper with variable speed. For warm background calibration, this chopper was replaced by a fixed-frequency (21.1 Hz) tuning fork chopper. The source output aperture exceeded the bolometer's field of view (FOV) at the separation distance of 73.2 cm, and was maintained at 23°C constant temperature. Figure 8 is a schematic of the bolometer bench test layout.

B.4 Chamber Calibration

Radiometric calibration was performed in the C^3, which is described in Ref. [6]. Because chamber radiometric power levels were lower than in the bench tests,

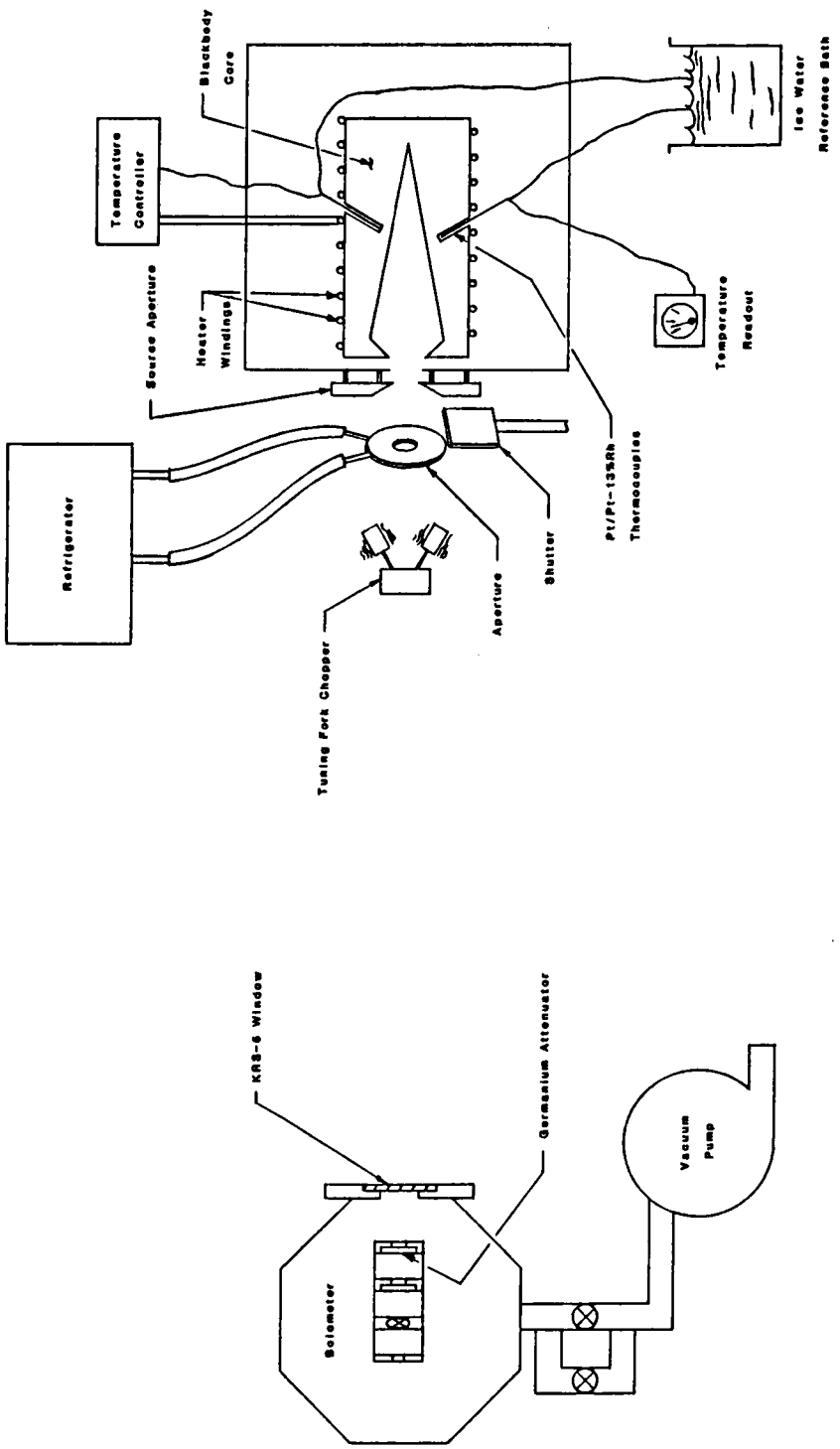


Figure 8. Bench Test Schematic.

both attenuating windows were removed to eliminate spectral effects. The bottom plate of the bolometer vacuum housing was also taken off to allow thermal linkage of the chamber 20K cold plate and the LN_2 cold shield. An independent insulating vacuum for the bolometer was not required, as the bolometer could utilize the chamber vacuum. Because the amplifier and internal calibrator driver would not function under cryogenic conditions, they were decoupled from the bolometer and placed outside the chamber.

The test source was the NBS-calibrated SIRS [1] with a 0.065-cm-diam aperture placed 25.94 cm from the bolometer element. The SIRS was mounted on a test fixture which had a shutter and a single-blade, 50-percent-duty chopper as integral components. The test fixture was provided with its own 20K helium cooling loop, and the SIRS was mounted with a 0.005-in. indium gasket to cool its housing conductively. Figure 9 shows a schematic of the test layout, while Fig. 10 is a photograph of the installation with callouts of the various components.

C. Instrumentation

Figure 11 shows the C^3 instrumentation system which is described in Ref. [9]. The spectrum analyzer and oscilloscope were added for the bolometer calibration, and

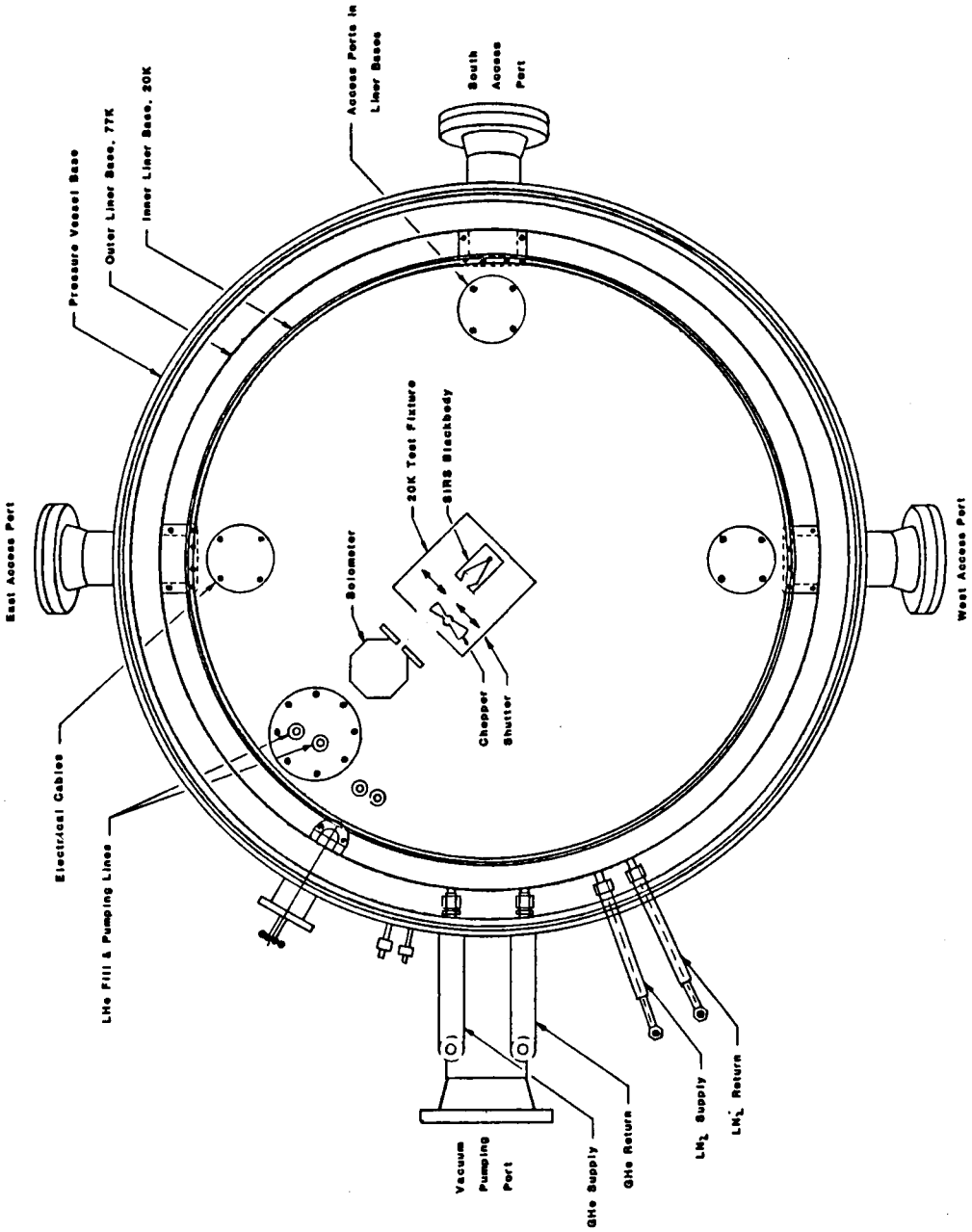


Figure 9. Chamber Calibration Schematic.

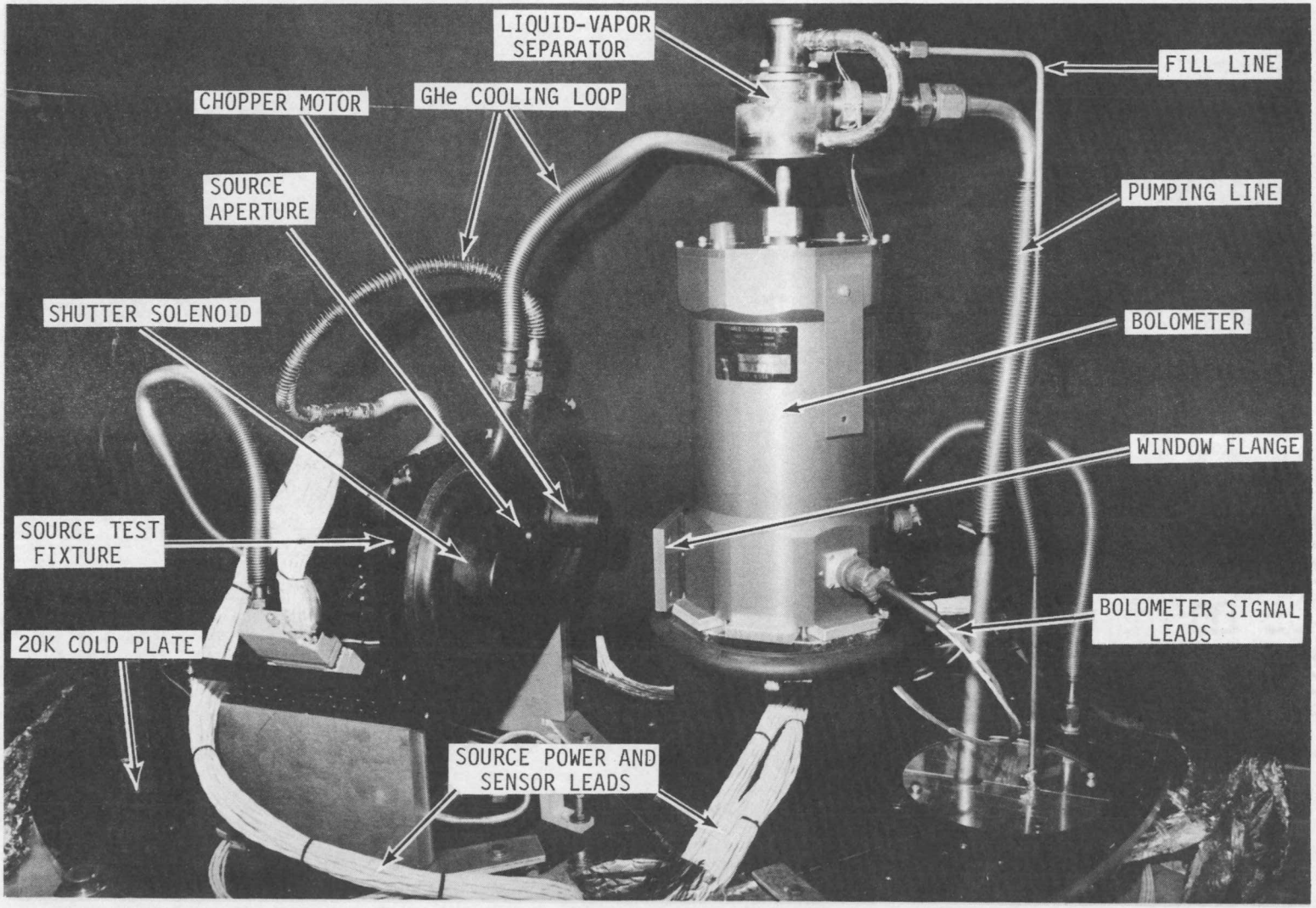


Figure 10. Bolometer Calibration Installation.

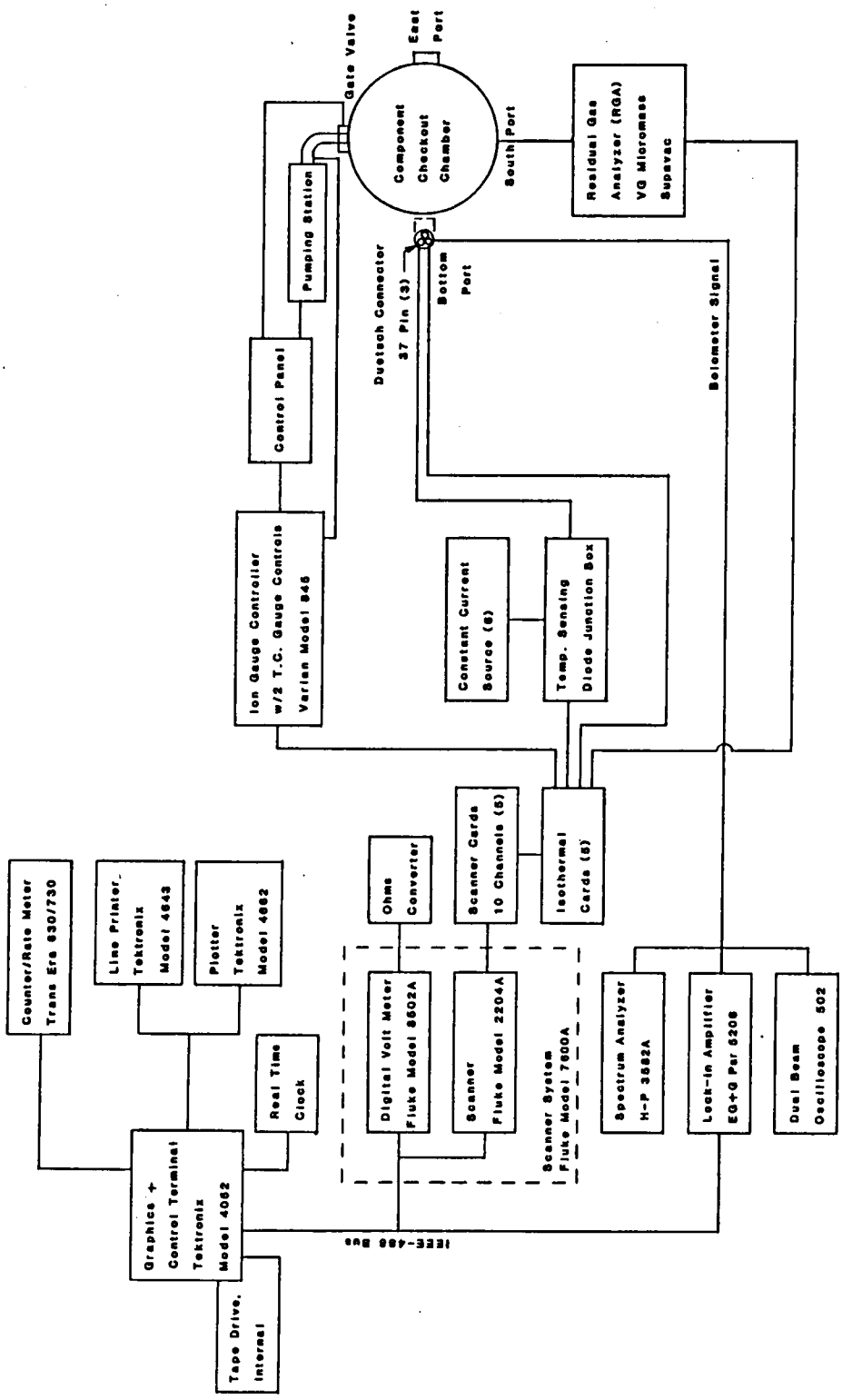


Figure 11. Chamber Instrumentation Schematic.

proved invaluable for noise diagnostics. The counter/rate-meter was another addition, which connected to the Tektronix® through a read-only-memory (ROM) slot. The Tektronix® 4052 terminal was the data processing center for this calibration and did most of its input interfacing through the digital voltmeter/scanner system. Figure 12 denotes the channel assignments on the multiplexing scanner.

D. Data Acquisition/Processing

Each data point of the bolometer calibration was the average of 500-point samples taken at 0.35-sec intervals. Calculation of bolometer responsivity used three such samples of data: source, tare, and internal calibrator readings. In addition, bolometer, SIRS, and chamber environmental parameters were recorded before and after each 500-point sample. Thus, a single calibration point represents over 1,600 readings.

Three programs were written for the Tektronix® terminal to facilitate data handling. The master calibration program contained six sections. These sections shared common function subroutines, but gave the program flexibility to handle different tests executed in various phases of the calibration. Each section had the capability to acquire, reduce, and display data, with options for hard copy and permanent magnetic tape storage. A second

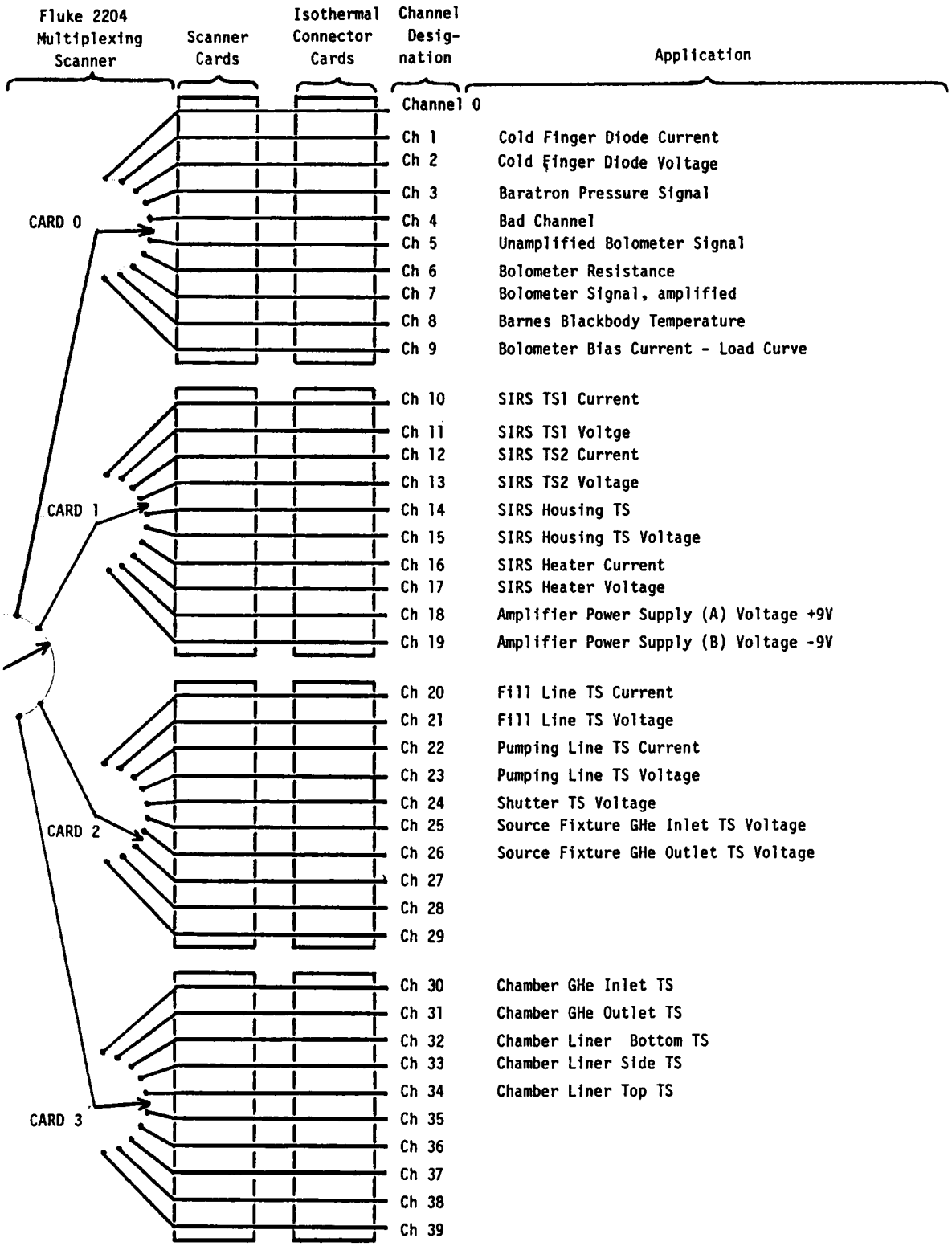


Figure 12. Bolometer Calibration Data Feeds.

program performed statistical analysis on large samples for quick-look data. The third was a plot program with user-friendly edit functions to display data in a high quality format. Each of these programs was written in structured form to allow use in future calibrations with slight modifications.

CHAPTER III

TEST DESCRIPTION

A. Bench Check

The objectives of the initial bench check were twofold: first, to shake down the bolometer and ensure that all systems were functioning; and second, to define those variables and parameters which would require special focus during the calibration.

Many difficulties were experienced and overcome during this work phase. A list of the more significant equipment failures includes: a short of the bolometer element caused by a flake of loose solder; a warped bolometer cold plate caused by overpressurization in the helium dewar; burned wires inside the bolometer; three op-amp failures in the bolometer amplifier, and intermittent performance from the internal calibrator LED. During this interval, the bolometer was twice returned to Infrared Laboratories for repairs. Another critical element was development of an effective helium fill procedure, described in Chapter II, Section B.1.

During the supercooling pumpdown, dewar pressure and bolometer resistance were measured; the vapor pressure was then used to calculate the cold plate temperature. A silicon diode was attached to the cold finger to verify

this temperature and to check for time lag as the bolometer mass cooled. No time lag was observed. The relationship of bolometer resistance to temperature was plotted, and resistance also provided an immediate functional check to ensure that another electrical short had not deactivated the bolometer.

Since this project was the first experience with the new bolometer, the effect of operating temperature was examined using the internal calibrator source. Lower temperature (i.e., lower dewar pressure) resulted in higher bolometer resistance and greater sensitivity (Fig. 13). Unfortunately, lower temperatures also consumed helium at a faster rate and thus reduced time available for testing. Twenty millimeters of helium vapor pressure (1.95K) produced satisfactory signal levels and was selected as the operating point for calibration work.

Another series of preliminary tests utilized the internal calibrator source to evaluate the impact of bias variation in the bolometer circuits. The amplifier circuit (Fig. 4, page 8) was particularly susceptible to battery drain and resulted in significant alteration of output signals. Precision 9-volt power supplies were substituted for the batteries and eliminated the problem.

Any variation in the bolometer bias would obviously produce a change in the output signal; however, power

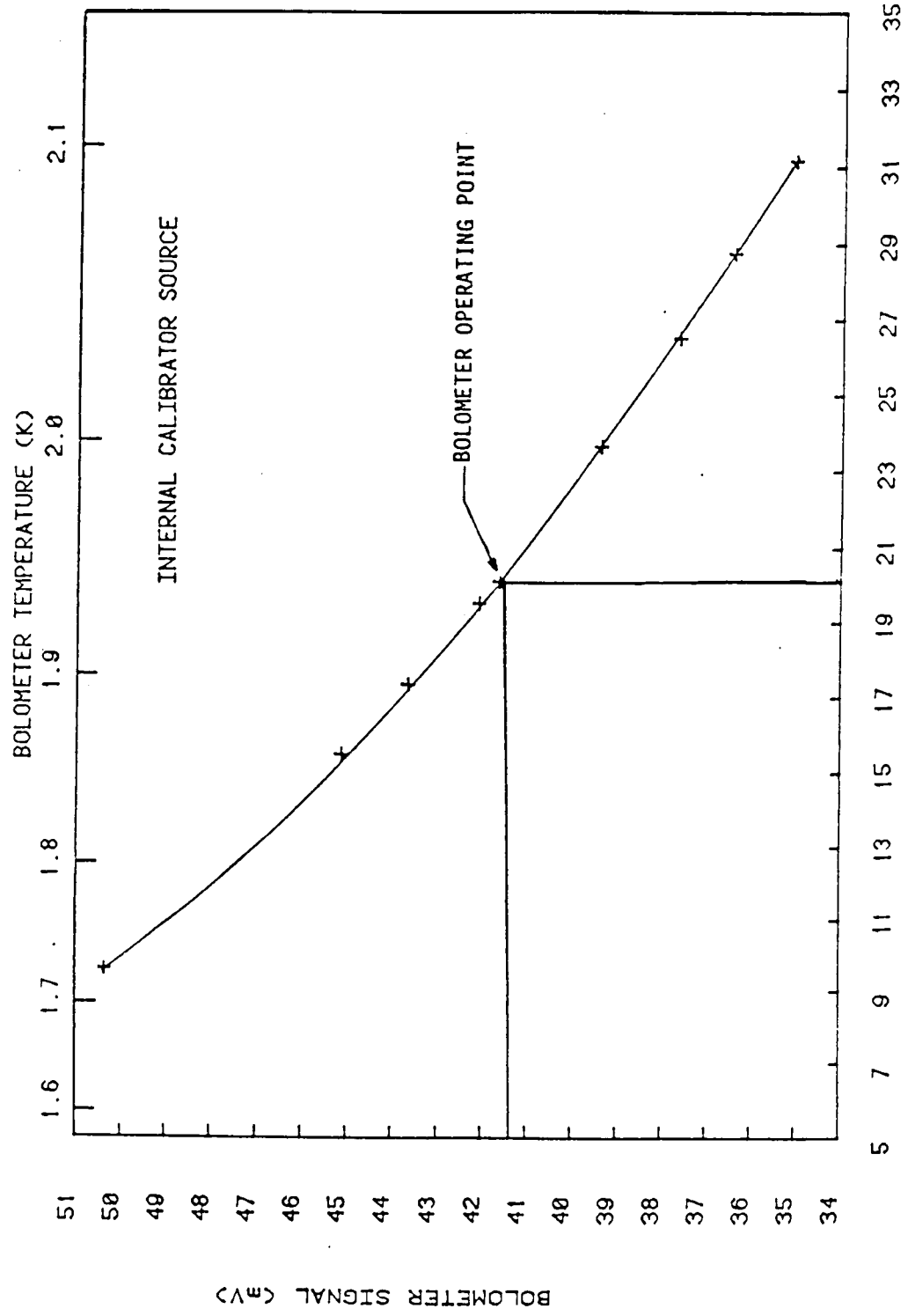


Figure 13. Bolometer Response to Operating Temperature.

consumption in this circuit was so small that the 9V battery could easily maintain adequate power levels for several days. A D.C. power supply was substituted temporarily, but the test produced ambiguous results. Source and tare signals increased when the bias changed to 7V, but internal calibrator signals went down. This issue could not be readily resolved, and since there was at least a potential problem with power supplies and 60-cycle noise, the calibration was conducted with battery bias.

No superficial effects were observed when internal calibrator batteries were low, and this circuit was also left "as-built" for the calibration. However, analysis of data taken late in the calibration with two new batteries produced higher signals. It is not clear whether the increase was a consequence of the new batteries or attributable to a change in the bolometer's operating state. Further tests will attempt to resolve this point and the issue of bolometer bias discussed above. If a problem is indicated, all batteries will be replaced with filtered precision power supplies.

B. Noise

Preliminary noise measurements were made during the bench check of the bolometer, and noise was also the first issue addressed once test conditions were reached in

the C^3. Spurious frequencies were identified with the spectrum analyzer and confirmed by serial deactivation and/or shielding. Noise contributions from an ion gage and an unshielded IEEE-488 cable were eliminated. Repositioning equipment and improved grounding also helped reduce broadband (0 to 25 kHz) noise levels an average of 10.8 dBV. Appendix A contains a more detailed discussion of noise measurements, and additional improvements are suggested in Chapter VI.

C. Load Curve

A load curve test defines the electrical throughput of the bolometer under cryogenic conditions. The test consists of two steps: variable bias voltage and variable bias current. Data are obtained by replacing the bias battery with a D.C. power supply. In step one, the input voltage is varied and the output signal voltage is recorded. Bias current is calculated as voltage-in minus voltage-out, divided by the load resistor. This test results in a plot of current through the bolometric region as a function of the voltage drop (output signal) across it.

Phase two has the bolometer looking at a constant IR source (or background). Bolometer bias voltage is fixed while bias current is varied and the output signal is recorded. Signal versus bias current is plotted, and

the optimum bias is found where the maximum signal occurs. When this bias is located on the plot from step one, a tangent to the curve at that point will define parameters which allow a theoretical bolometer responsivity to be calculated.

References [5] and [10] discuss load curve theory and reach the common conclusion that the estimated responsivity is always higher than the experimental value. For this reason, and because battery power would not allow regulation of the bias current, the second part of the load curve test was not performed. If the bias battery is replaced with a power supply for future bolometer work, the full load curve test should be run to optimize bias conditions. Figure 14 shows a typical response to part one (voltage variation), which is used as a daily indicator of the bolometer's uniform performance. The slight scatter in the data is due to a bad dashpot in the power supply; however, with the aforementioned purpose such deviation is insignificant.

Load curve results are seen in Fig. 15 along with manufacturer's data. While the difference appears large, it causes insignificant variation in the calculated responsivity. With a bias of 0.4 amps (the optimum current from manufacturer's data), all three curves produce

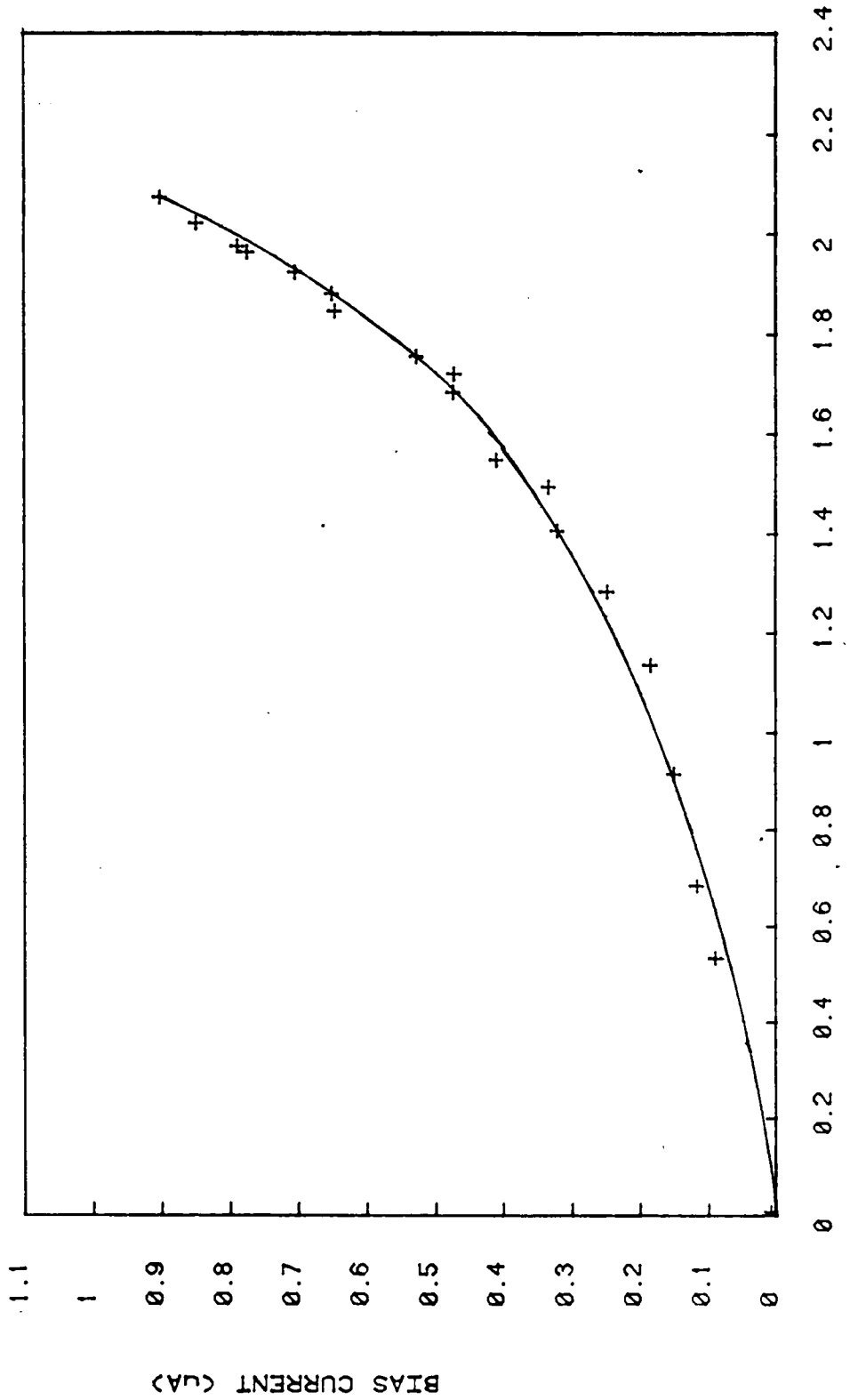


Figure 14. Typical Load Curve.

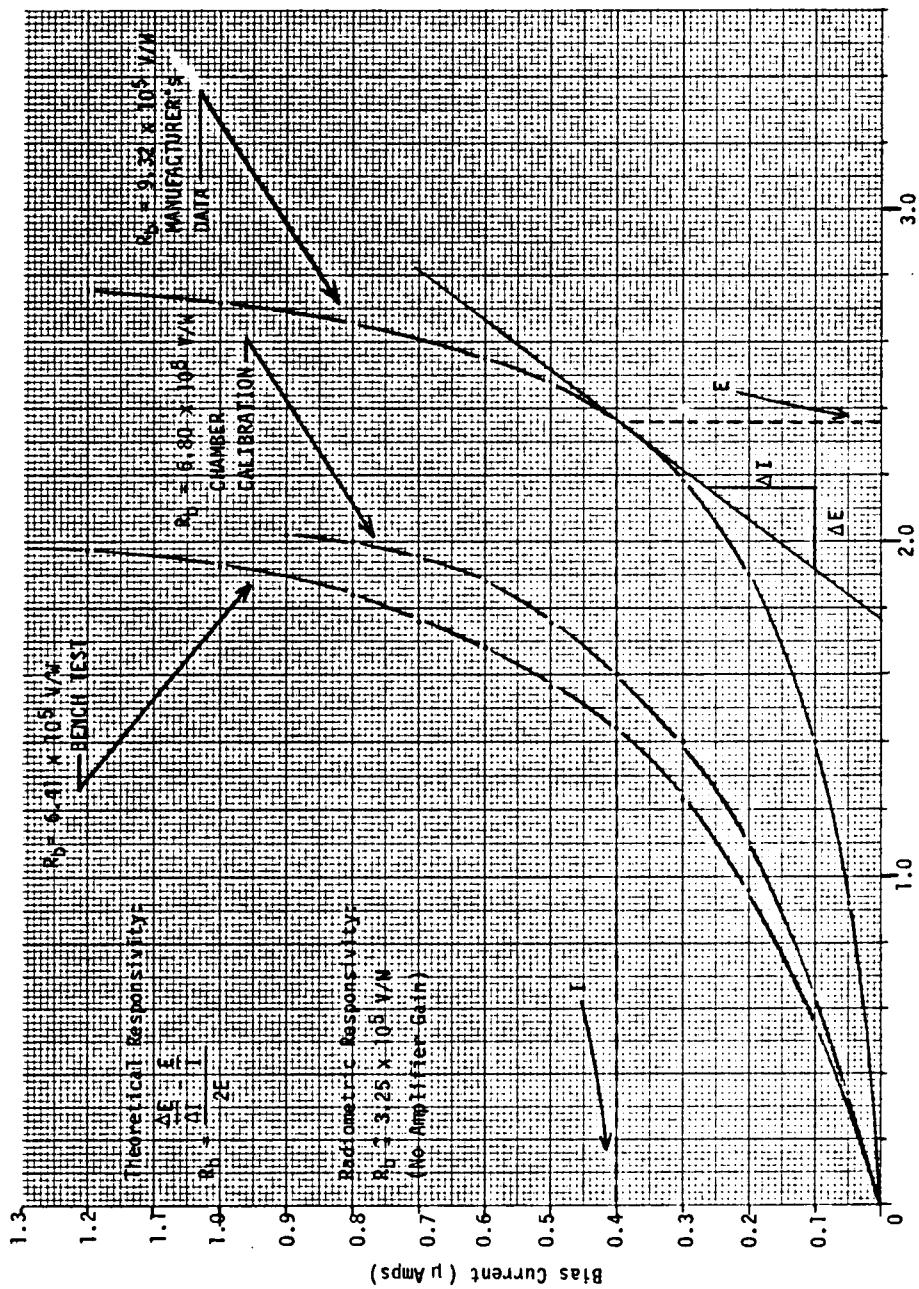


Figure 15. Bolometer Load Curves.

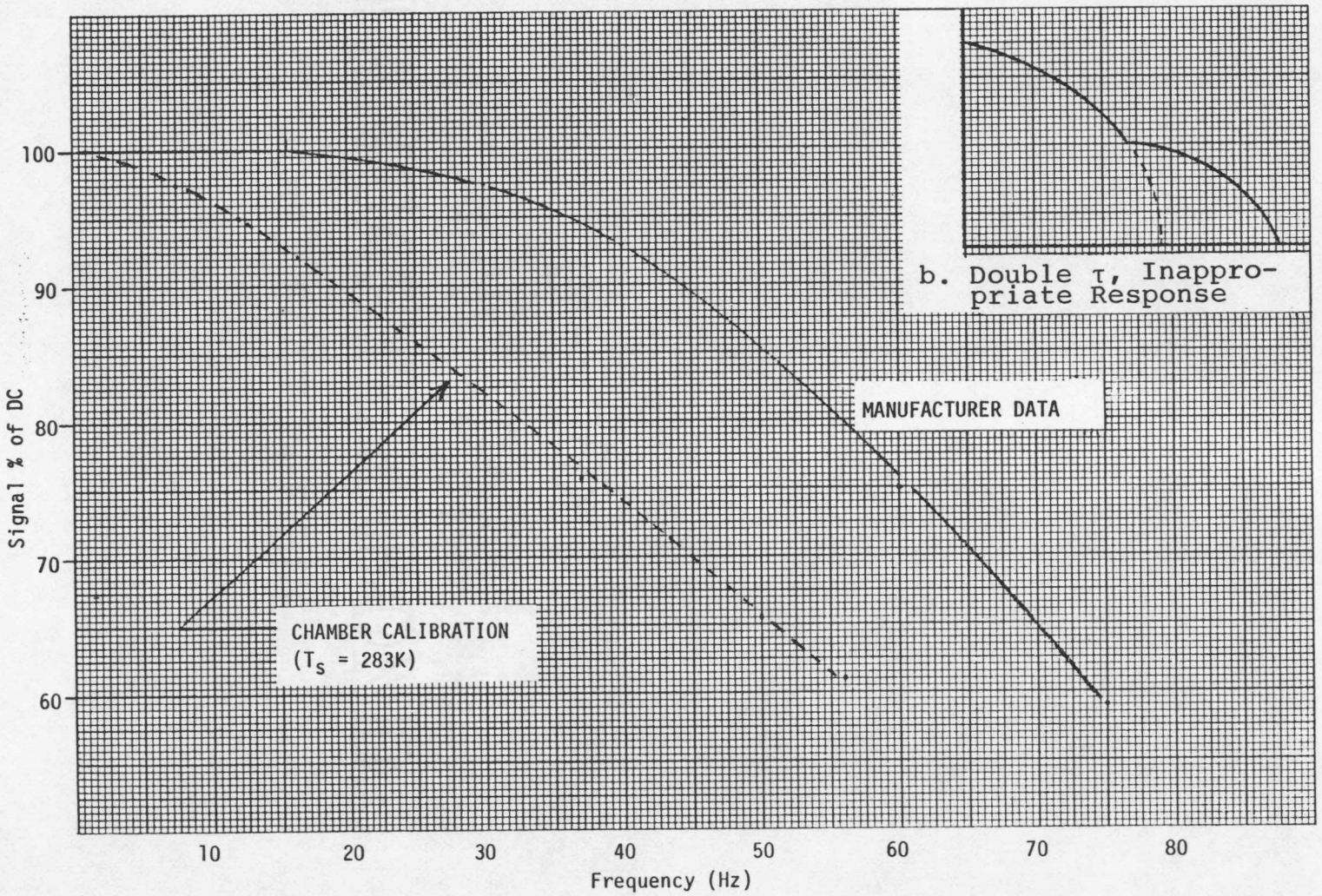
responsivities in the same order of magnitude as the value obtained during radiometric calibration.

D. Frequency Response

The frequency response test measures the bolometer's signal output when incoming radiation is chopped at different speeds. Results are expected to be nonlinear (at higher frequencies, the bolometer element has less time to reach thermal equilibrium). The objectives of the test are to ensure that the bolometer does not have a dual time constant and to select a calibration frequency that will maximize the output signal while avoiding regions of noise and chopper instability.

Instability is device-dependent. One chopper may run irregularly at 27 Hz, while another unit may have difficulty in a totally different range. Noise frequencies may come from the test setup or may relate to other activities in the chamber area. Frequencies with a harmonic relationship to 60 Hz must obviously be avoided.

Figure 16a illustrates results from a typical calibration frequency test and similar data from the bolometer manufacturer. The bolometer appears to be more sensitive to frequency variation than expected; however, there is no hint of a dual time constant response (Fig. 16b).



a. Experimental Results

Figure 16. Bolometer Frequency Response.

During radiometric calibration, frequency was not consciously varied, and future use of the bolometer for null calibration will utilize a fixed-frequency tuning fork chopper. A chopper frequency of 16 Hz was chosen for bolometer calibration since it satisfied all of the criteria discussed above. From Fig. 16a, a correction factor of 0.69 percent per Hertz was derived and applied to any data taken at other than 16 Hz using Eq. (1):

$$f_C = 0.0069\ (16-F)\ , \qquad (1)$$

where

f_C = proportional frequency correction,

0.0069 = experimentally determined correction factor,

16 = standard chopping frequency,

F = frequency at which the data were taken.

E. Chamber Calibration

Radiometric calibration consisted of three types of measurements: bolometer response to a calibrated source, bolometer measurement of chopper tare, and bolometer response to the internal calibrator (IC) source. The signal response to the SIRS was the principal measurement; tare and internal calibrator readings produced correction factors.

Chopper tare quantifies an additional radiant load and is best explained in conjunction with Fig. 17. The calibrated source signal is produced by the bolometer alternately viewing the SIRS and the chopper blade. This A.C. signal is measured by the EG&G amplifier, locked on to a reference pulse from the chopper driver. Signal magnitude is equivalent to the difference between SIRS blocked and unblocked; however, the total energy on the detector is from the SIRS and any other object above 20K. Because of the rotational friction and difficulty in cooling, the chopper is always warmer than 20K. To measure chopper tare, the SIRS is covered by the 20K shutter and the EG&G records the difference between warm chopper and cold shutter. Because this waveform is 180 deg out of phase with the reference pulse, the tare signal has a negative value. Signal correction by subtracting (a negative) tare is therefore equivalent to adding its absolute value. Chopper tare correction thus makes the bolometer signal correspond to the total radiant load on the detector.

The internal calibrator has a fixed size and separation from the bolometer detector, and its output is assumed to be constant from day to day. Since IC chopping is done electrically at a fixed frequency, there is no tare or frequency response to consider. Therefore, any change in the IC signal will define a small shift in the bolometer's operating characteristics. Since bias

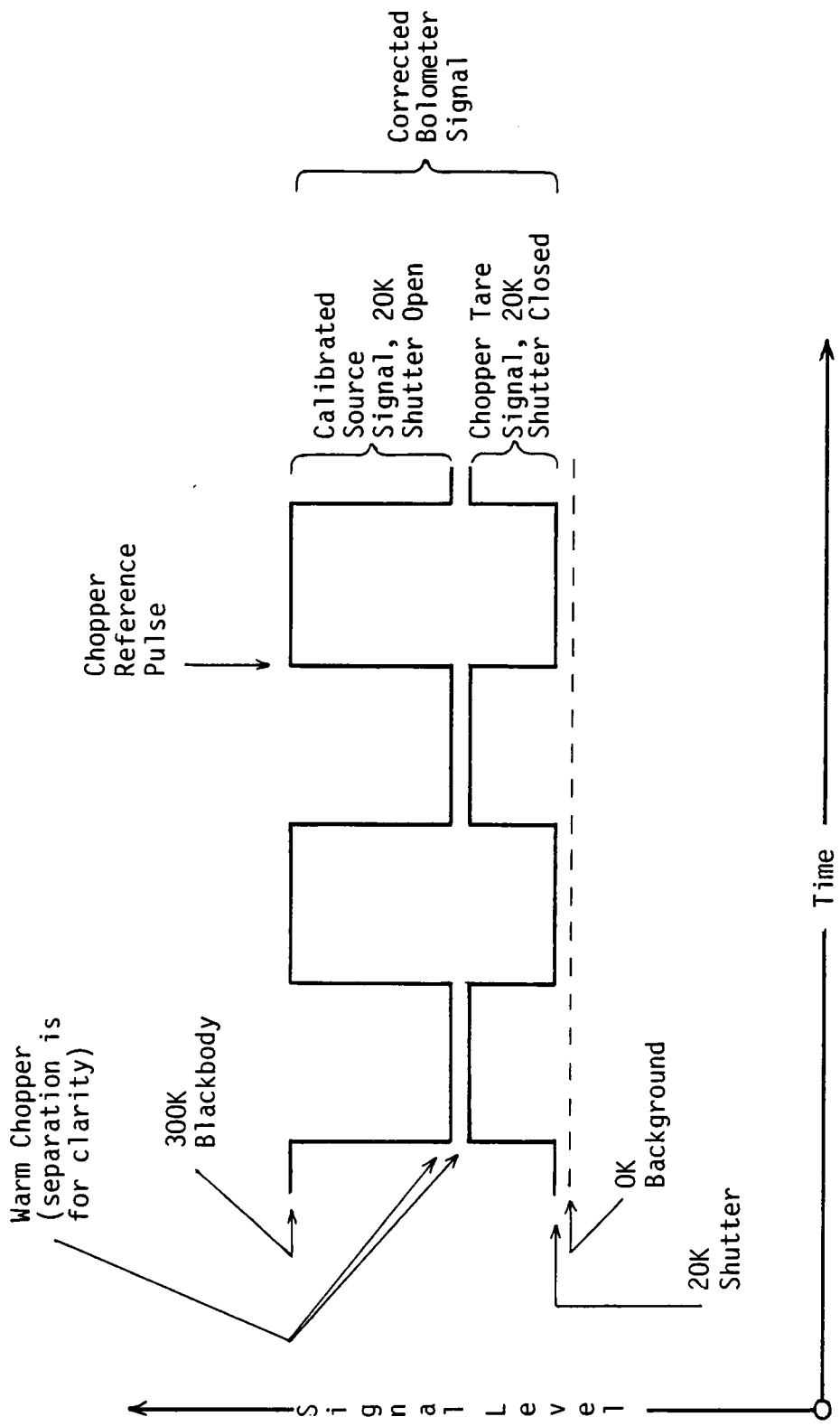


Figure 17. Chopper Tare Correction.

voltage/current are carefully maintained, such a shift will most probably be due to bolometer operating temperature (helium dewar pressure). Correction to the calibrated source signal is made indirectly, by normalizing to the average internal calibrator signal at 20-mm vapor pressure.

Each calibration point incorporated the three data types just described. The test sequence involved stabilizing the SIRS temperature and recording IC response, chopper tare, and response to the SIRS. Data samples included 500 readings at each point, and the average value was used for computation. Plotting and analysis of data were carried out while the SIRS was stabilizing at the next temperature. The range of source temperatures over which the bolometer was exercised was 275 to 390K, the verifiable limits imposed by the NBS calibration [1].

CHAPTER IV

RESULTS

Radiometric calibration of the bolometer was performed in the C^3 from March 1 through March 13, 1984. Calibration measurements are found in Table 1. Additional IC readings were taken during this interval, and Fig. 18 shows all such measurements in the neighborhood of 20-mm dewar pressure. As mentioned in Chapter III, Section E, IC response was used to normalize the bolometer response, and the data in Fig. 18 justify such an approach. The mean signal value at the selected operating point is 41.3 mV, and there is a clear relationship between IC response and small variations in dewar pressure.

A. Data Reduction and Corrections

The figure of merit chosen to evaluate the bolometer was responsivity, which is the RMS signal voltage per unit RMS radiant power incident upon the detector,

$$R_b = \frac{E_b}{P} \left(\frac{mV}{nW} \right) . \qquad (2)$$

Bolometer signal reduction, first alluded to in Chapter III, Section E, is written:

$$E_b = (E_S + E_T) \left(\frac{41.3}{E_{IC}} \right) (1 + fc) , \qquad (3)$$

Table 1. Bolometer Data

Date	Point No.	Source Temperature (K)	Frequency (Hz)	Signals		
				Source (mV)	Tare (mV)	Internal Calibrator (mV)
3/6/84	1	283.31	16.2	89.15	13.90	41.52
	2	283.30	13.0	90.71	15.25	41.49
	3	283.31	16.2	84.08	19.25	41.46
	4	299.47	16.2	105.90	19.21	41.46
	5	319.51	16.2	138.01	19.20	41.53
	6	339.86	16.2	176.46	18.23	41.23
	7	360.21	16.2	218.79	17.92	41.18
	8	383.32	16.2	279.03	17.68	41.07
	9	383.34	16.2	278.40	17.96	40.90
	10	360.36	16.2	219.68	17.80	41.01
	11	339.58	16.35	174.32	17.63	41.12
	12	319.42	16.3	136.91	17.54	41.05
	13	299.52	16.25	105.24	17.80	41.00
	14	282.77	16.3	83.96	15.34	40.40

Table 1. (continued)

Date	Point No.	Source Temperature (K)	Frequency (Hz)	Signals		
				Source (mV)	Tare (mV)	Internal Calibrator (mV)
3/7/84	15	282.79	16.3	94.86	7.11	41.23
	16	282.79	16.3	94.70	7.28	41.23
	17	299.51	16.3	116.46	8.48	41.34
	18	319.57	16.3	147.59	9.97	41.46
	19	339.64	16.3	184.99	10.06	41.47
	20	360.04	16.3	231.63	9.53	41.49
	21	359.95	16.3	231.58	10.18	41.49
	22	383.18	16.2	290.71	10.68	41.50
	23	360.10	16.3	229.92	11.30	41.53
	24	339.85	16.3	185.32	10.83	41.60
	25	339.84	16.2	185.17	11.01	41.61
	26	339.77	16.2	185.09	11.17	41.62
	27	319.60	16.3	145.61	11.97	41.65
	28	299.53	16.3	114.75	10.95	41.63
	29	282.80	16.3	91.49	11.44	41.62

Table 1. (continued)

Date	Point No.	Source Temperature (K)	Frequency (Hz)	Signals		
				Source (mV)	Tare (mV)	Internal Calibrator (mV)
3/8/84	30	282.81	16.3	102.24	1.62	41.70
	31	282.79	16.2	94.34	9.11	41.70
	32	282.80	16.2	93.97	9.08	41.70
	33	299.52	16.2	118.13	8.73	41.53
	34	324.59	16.2	158.10	10.46	41.34
	35	350.12	16.2	209.00	11.39	41.15
	36	375.36	16.2	266.83	10.70	40.90
3/9/84	37	282.92	16.2	100.76	2.34	41.50
	38	382.60	16.2	291.03	10.06	41.00
	39	383.23	16.2	292.02	9.64	41.00
	40	383.14	16.6	283.85	15.19	40.95
	41	283.83	16.6	88.17	8.62	38.15
3/12-13/84	42	391.72	16.6	187.32	146.37	42.35
	43	391.20	16.6	273.94	55.71	41.56
	44	283.91	16.6	78.09	27.15	42.14

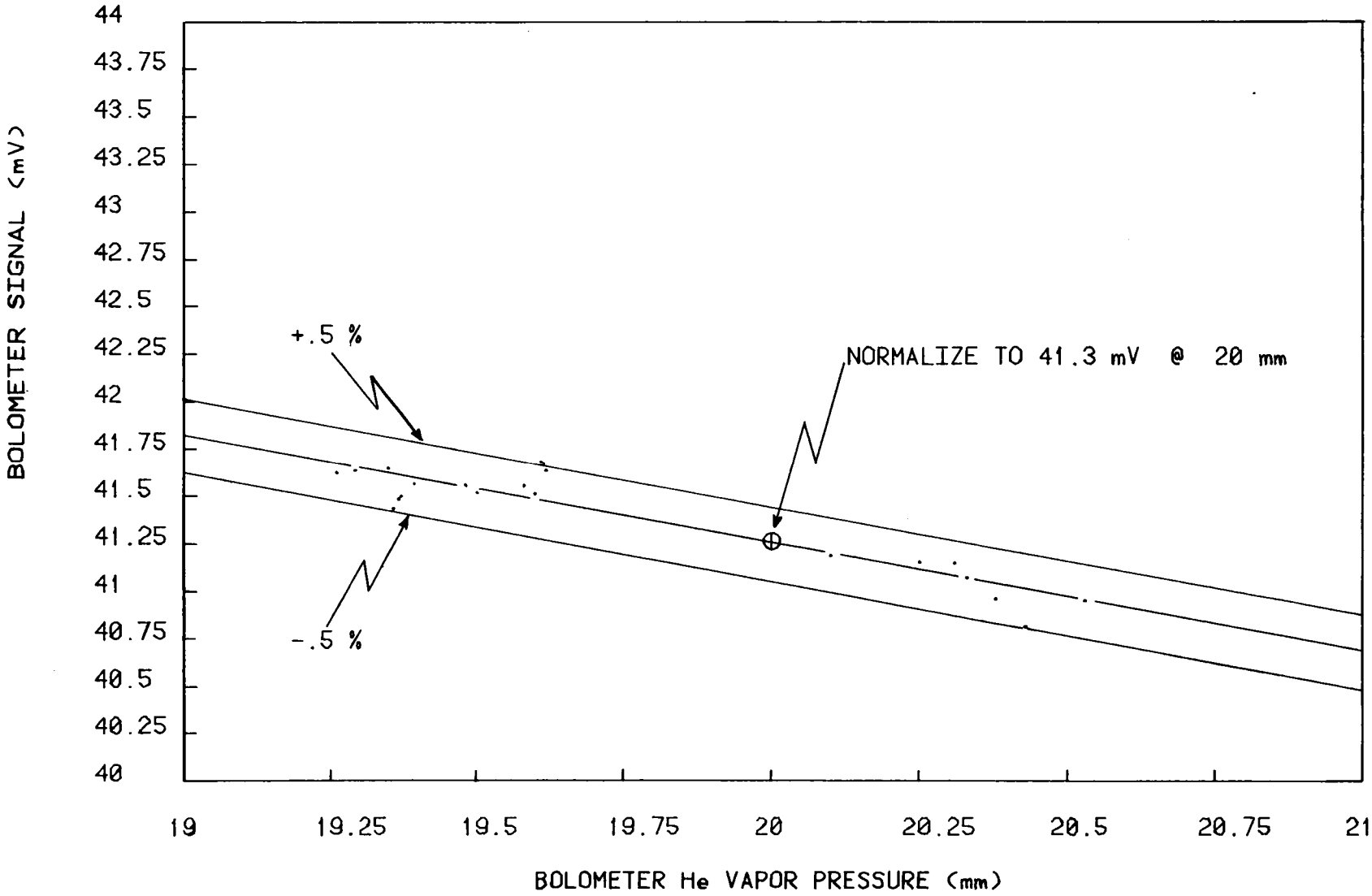


Figure 18. Internal Calibrator Response to Small Fluctuations in Dewar Pressure.

where

E_b = corrected bolometer signal in millivolts,

E_S = bolometer signal from the SIRS
E_T = chopper tare signal
E_{IC} = internal calibrator signal
} RMS millivolt signals recorded by the EG&G 5206 lock-in amplifier,

41.3 = internal calibrator normal response with 20-mm helium vapor pressure (from Fig. 18),

fc = frequency correction from Eq. (1).

Power absorbed by the bolometer element when exposed to the SIRS is given by:

$$P = \frac{1}{2.22} (\alpha\varepsilon\sigma T^4)\left(\frac{A_S A_b}{\pi D^2} \right), \qquad (4)$$

where

2.22 = conversion factor (RMS power),

α = absorptivity of the painted bolometer surface (0.96),

ε = emissivity of the SIRS (1.0),

σ = Stefan-Boltzmann constant (5.670×10^{-12} W/cm^2 K^4),

T = SIRS blackbody temperature in Kelvins (from NBS calibration),

A_S = area of source aperture (3.299×10^{-3} cm^2) (corrected for thermal contraction at 20K),

A_b = area of bolometer (0.012192 cm^2) (corrected for thermal contraction at 20K),

D = source/detector separation (26.41236 cm)
(corrected for thermal contraction at 20K).

In Eq. (4), the second term is the Boltzmann law for transfer of radiant energy, and the third term is the experimental view factor. Insertion of the appropriate constants into Eq. (4) will reduce the power calculation to:

$$P = 4.725 \times 10^{-20} (T^4) \quad . \tag{5}$$

Combining Eqs. (3) and (5) in the form of Eq. (2) yields the simplified responsivity calculation:

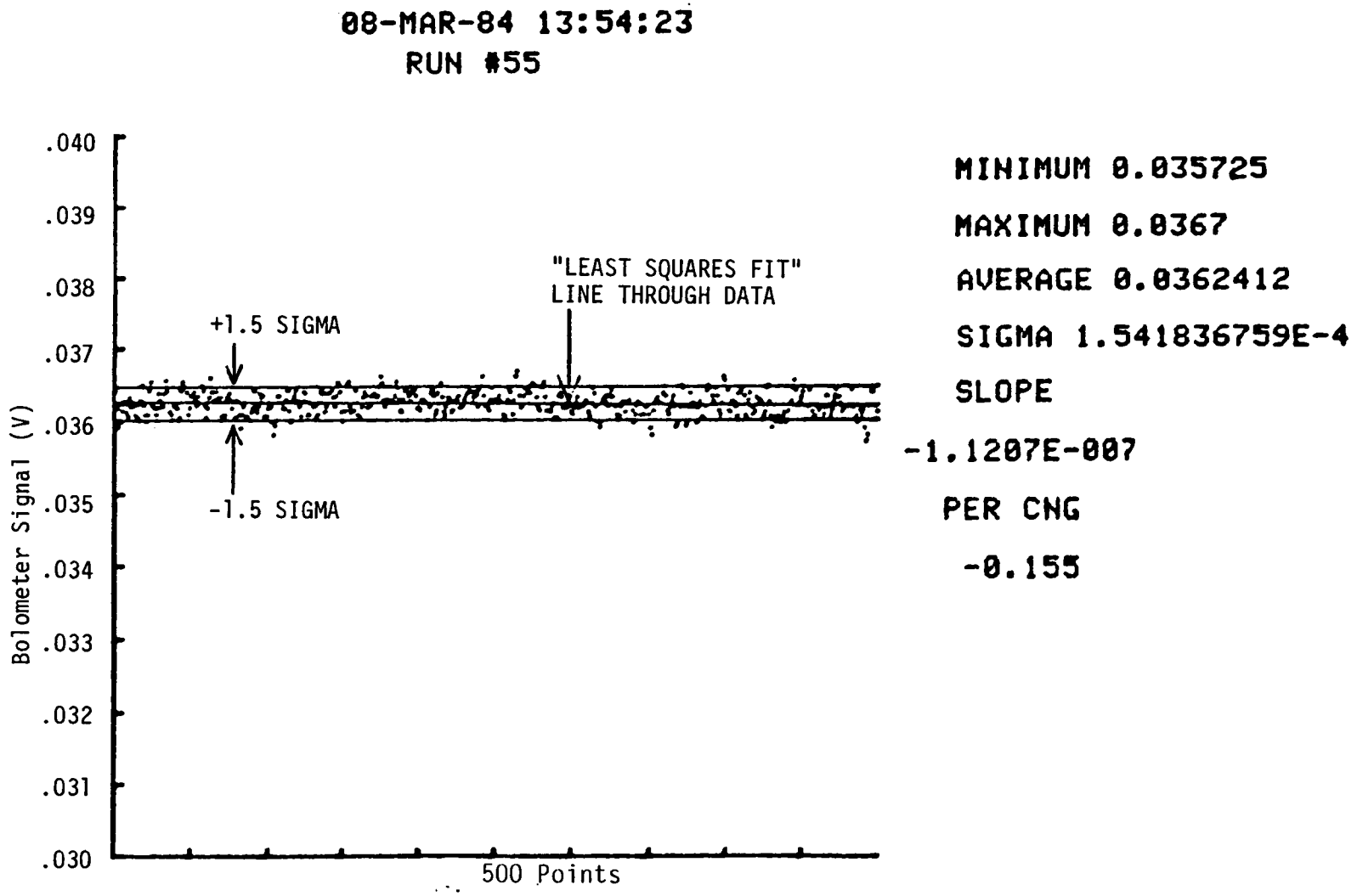
$$R_b = \frac{8.7407 \times 10^{17}(E_S + E_T)(1 + f_C)}{T^4 \ (E_{IC})} \left(\frac{mV}{n\bar{W}} \right) . \tag{6}$$

All dimensions in Eq. (4) were corrected for thermal contraction according to approved methods [11], and T is the calibrated radiance temperature from NBS [1]. Samples of these calculations are found in Appendix B.

In previous work at AEDC when the SIRS blackbody has been used, a diffraction correction has been applied to the power calculation [1,12]. Careful analysis reveals that the diffraction loss is dependent only on the source geometry and was included in the NBS calibration of the SIRS. Reference [13] confirms that to apply the diffraction correction again would be an error.

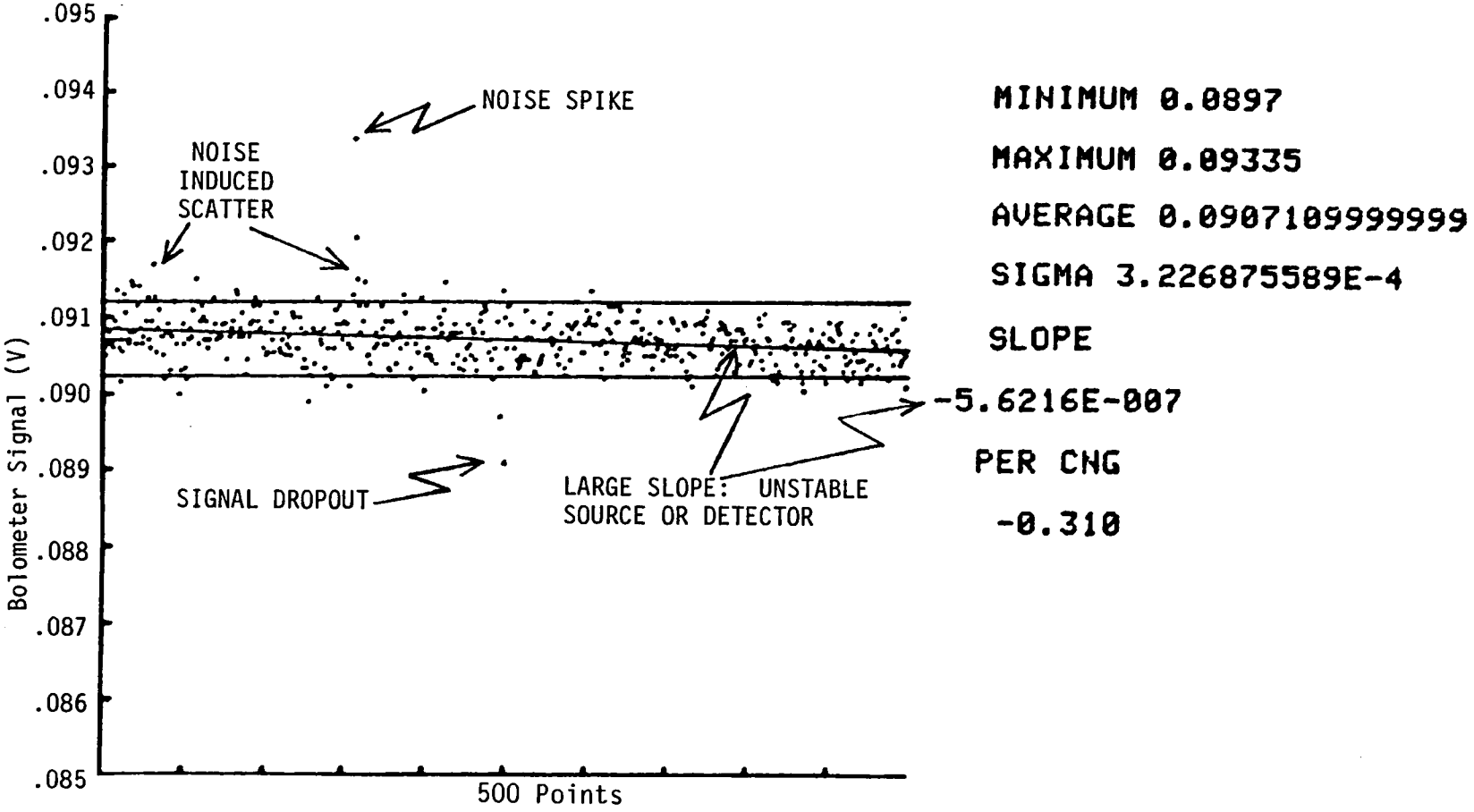
Five hundred-point data samples were first plotted as shown in Fig. 19a. Bracketing lines around the data were arbitrarily drawn at ± 1.5 standard deviations; maximum, minimum, average, and slope values were also computed. These plots allowed quick visual identification of anomalies including data scatter, cyclic variation, noise spikes, and signal dropout points (Fig. 19b). The average value for each sample was then inserted at the appropriate location in Eqs. (3), (5), and (6). Table 2 presents the corrected numerical values, and Figs. 20a through 20e show daily responsivity plots.

On March 9, 12, and 13, calibration was done by an alternate method. Sample size was smaller (50 points/sample), but samples were taken in close time proximity. The SIRS was heated to 400K; then the heater power was turned off and the source began cooling slowly at about one Kelvin per minute. Bolometer-source response (E_S) was recorded every 60 seconds, and at each fifth interval the chopper tare (E_T) was read. Without applying frequency or internal calibrator corrections, signal versus source temperature was plotted in Fig. 21. While the numeric uncertainty of any one of these points may be greater with the small sample size, the scatter of the entire data set is less. Five hundred-point samples at wide time intervals represent discrete occurrences, with the possibility of instrument or environment perturbations in the interim.



a. Good Data Sample (typical)

Figure 19. Data Sample Diagnostic Plots.



b. Poor Data Sample with Problems Indicated (atypical)

Figure 19. (continued)

Table 2. Corrected Results

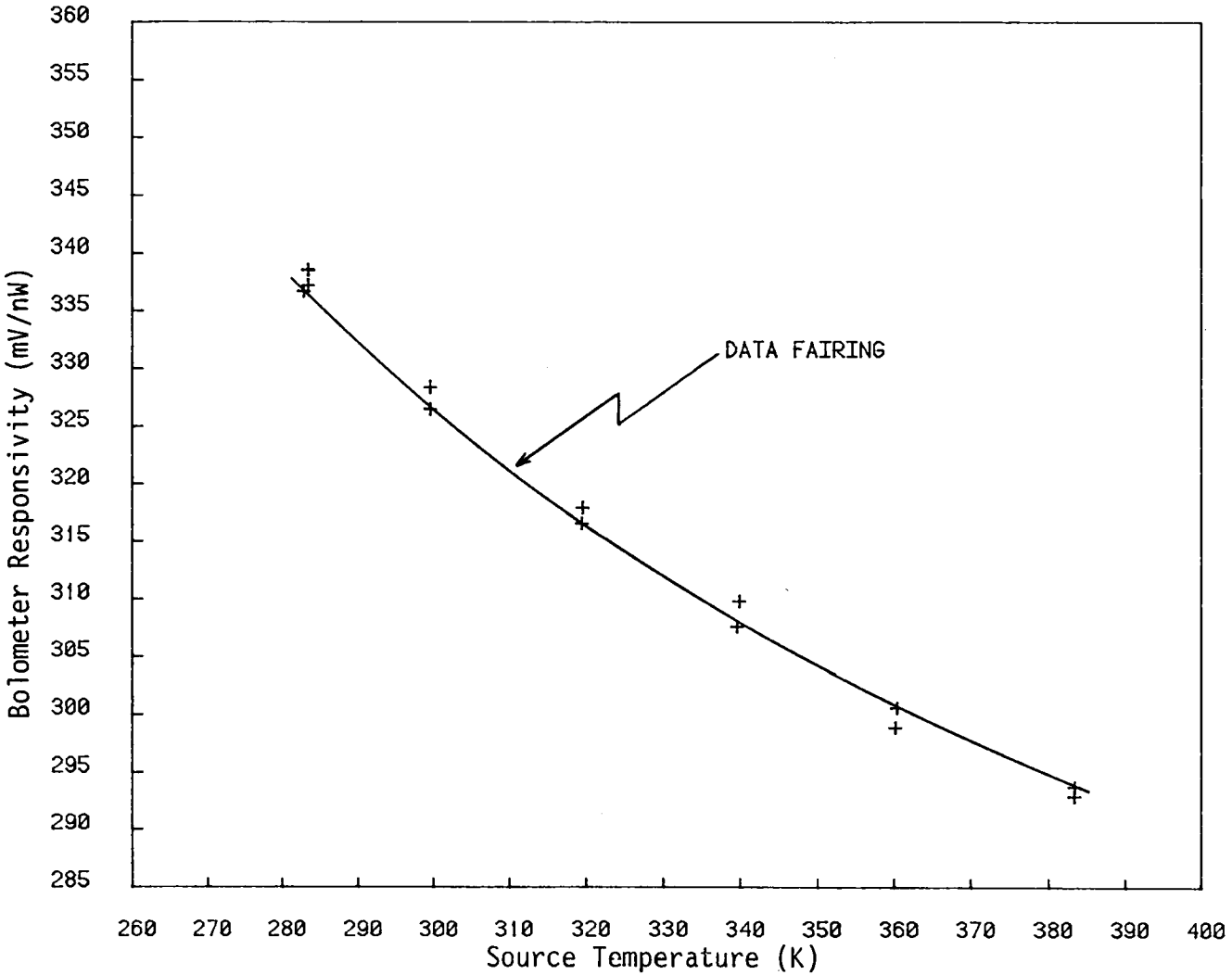
Date	Point No.	Source Temperature (K)	Corrected Signal (mV)	Corrected Power (nW)	Bolometer Responsivity (mV/nW)
3/6/84	1	283.31	102.65	0.30440	337.21
	2	283.30	103.04	0.30436	338.56
	3	283.31	103.07	0.30440	338.61
	4	299.47	124.80	0.38003	328.40
	5	319.51	156.56	0.49242	317.93
	6	339.86	195.29	0.63038	309.80
	7	360.21	237.73	0.79547	298.85
	8	383.32	298.78	1.02011	292.89
	9	383.34	299.67	1.02032	293.70
	10	360.36	239.49	0.79680	300.56
	11	339.58	193.26	0.62830	307.58
	12	319.42	155.71	0.49187	316.57
	13	299.52	124.15	0.38028	326.48
	14	282.77	101.72	0.30209	336.73

Table 2. (continued)

Date	Point No.	Source Temperature (K)	Corrected Signal (mV)	Corrected Power (nW)	Bolometer Responsivity (mV/nW)
3/7/84	15	282.79	102.36	0.30217	338.74
	16	282.79	102.36	0.30217	338.74
	17	299.51	125.08	0.38023	328.95
	18	319.57	157.28	0.49279	319.15
	19	339.64	194.65	0.62875	309.59
	20	360.04	240.55	0.79397	302.97
	21	359.95	241.15	0.79318	304.03
	22	383.18	300.35	1.01862	294.86
	23	360.10	240.38	0.79450	302.56
	24	339.85	195.14	0.63030	309.59
	25	339.84	194.99	0.63023	309.39
	26	339.77	195.02	0.62971	309.70
	27	319.60	156.58	0.49298	317.62
	28	299.53	124.96	0.38033	328.56
	29	282.80	102.35	0.30222	338.66

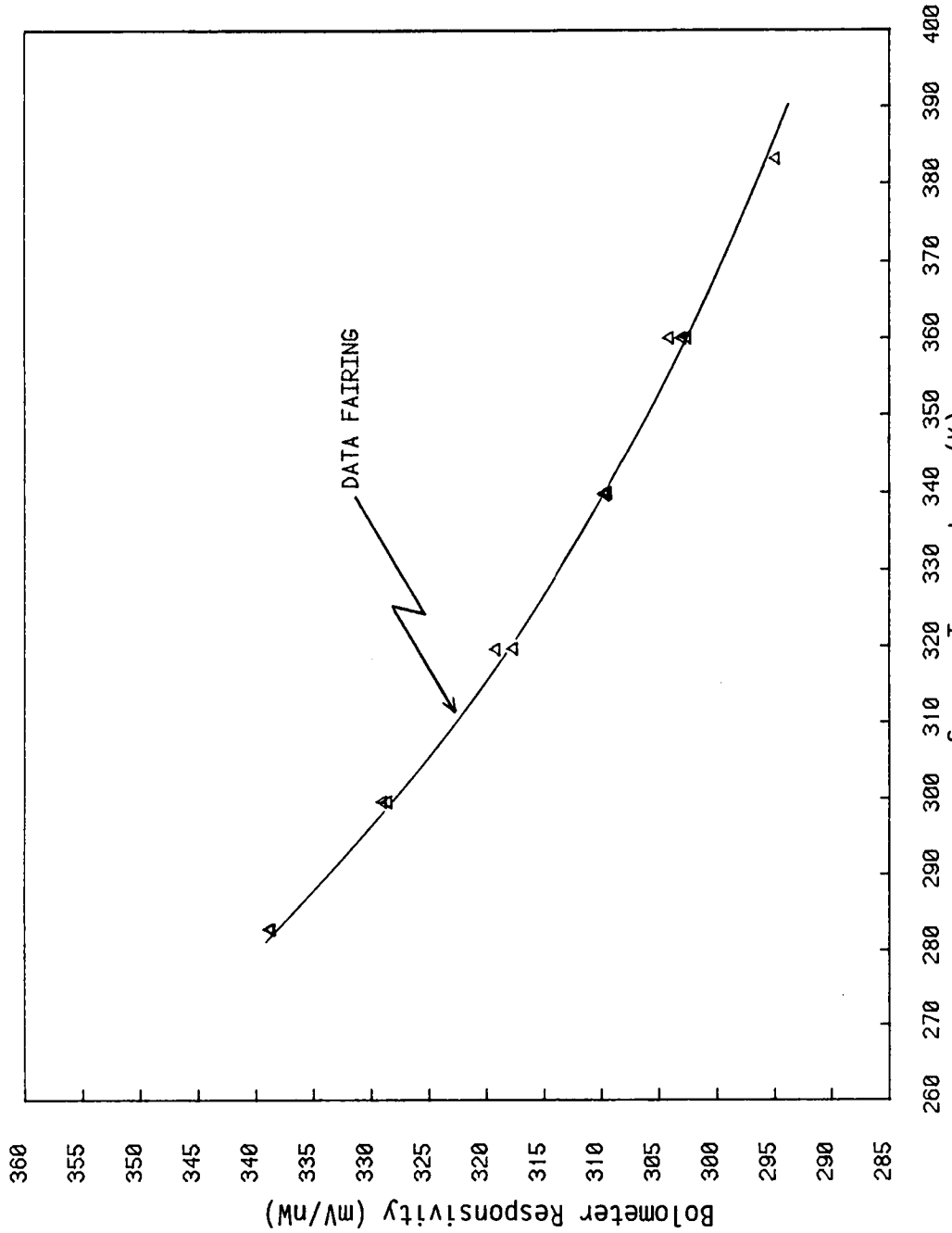
Table 2. (continued)

Date	Point No.	Source Temperature (K)	Corrected Signal (mV)	Corrected Power (nW)	Bolometer Responsivity (mV/nW)
3/8/84	30	282.81	103.08	0.30226	341.02
	31	282.79	102.60	0.30217	339.54
	32	282.80	102.20	0.30222	338.17
	33	299.52	126.33	0.38028	332.21
	34	324.59	168.63	0.52450	321.51
	35	350.12	221.50	0.71002	311.96
	36	375.36	280.63	0.93798	299.18
3/9/84	37	282.92	102.74	0.30273	339.39
	38	382.60	303.71	1.01247	299.97
	39	383.23	304.29	1.01915	298.57
	40	383.14	302.84	1.01820	297.43
	41	283.83	105.22	0.30664	343.12
3/12-13/84	42	391.72	326.76	1.11251	293.72
	43	391.20	328.94	1.10662	297.25
	44	283.91	103.57	0.30699	337.37



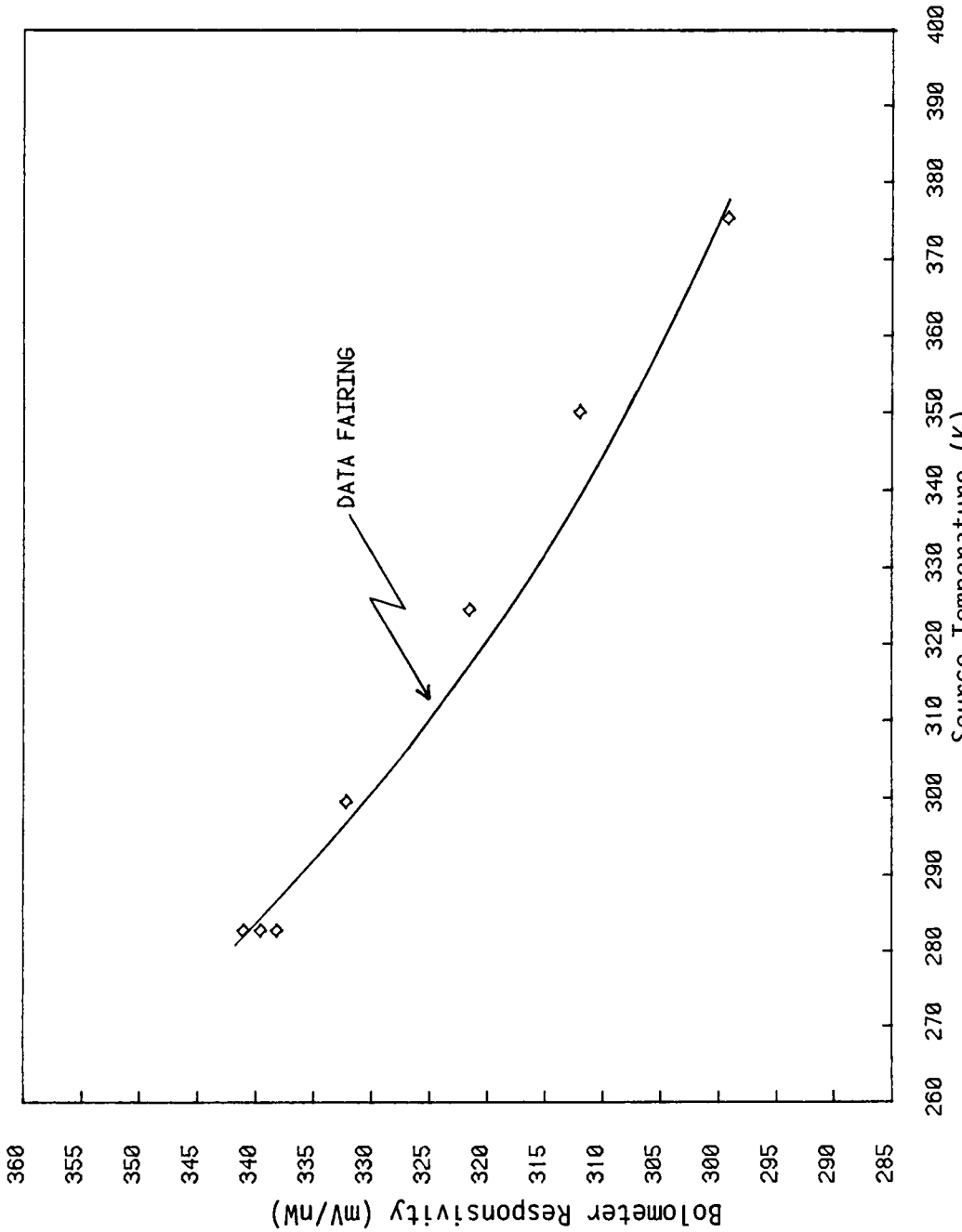
a. March 6 Responsivity

Figure 20. Bolometer Calibration Results, Data Obtained by Standard Method.



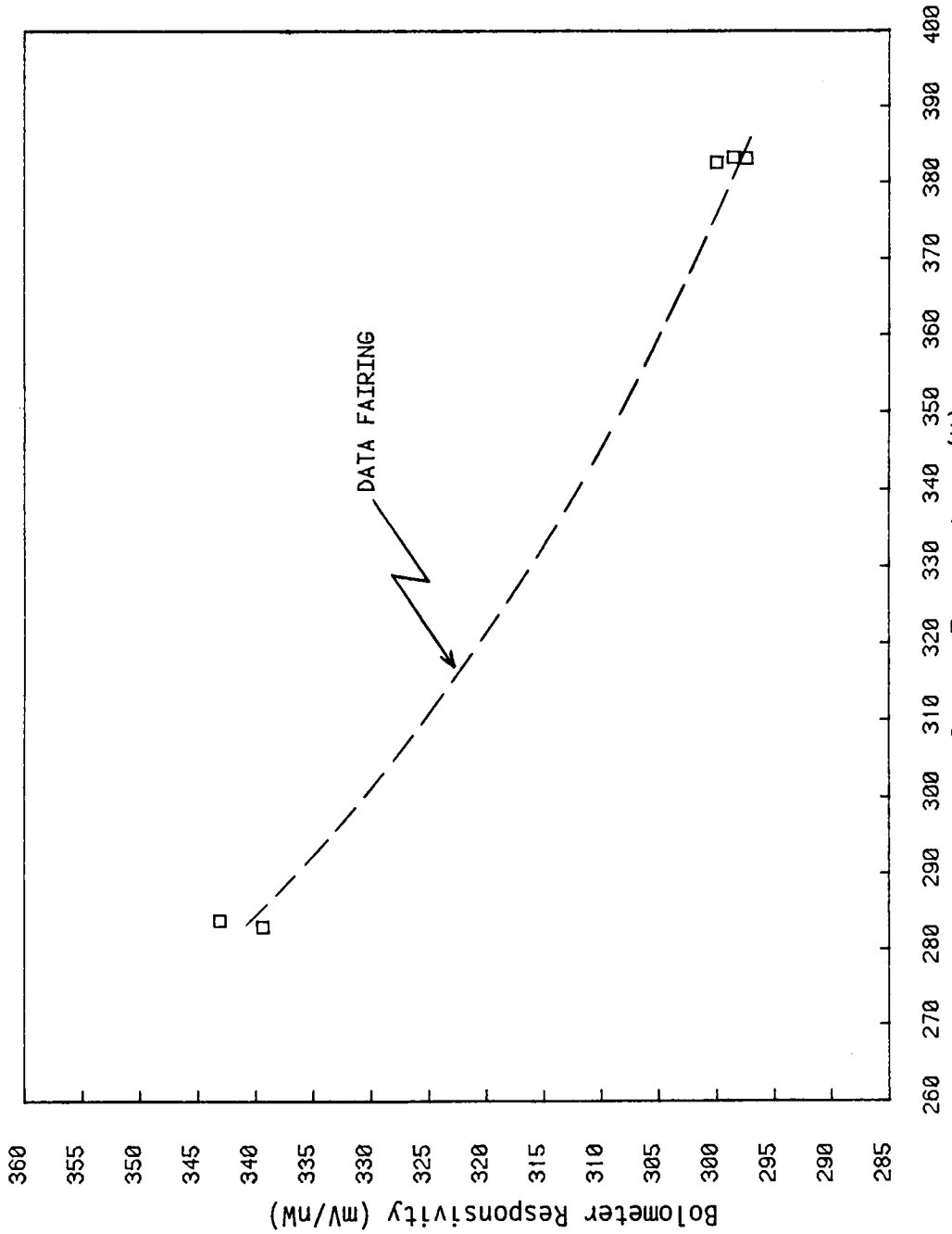
b. March 7 Responsivity

Figure 20. (continued)



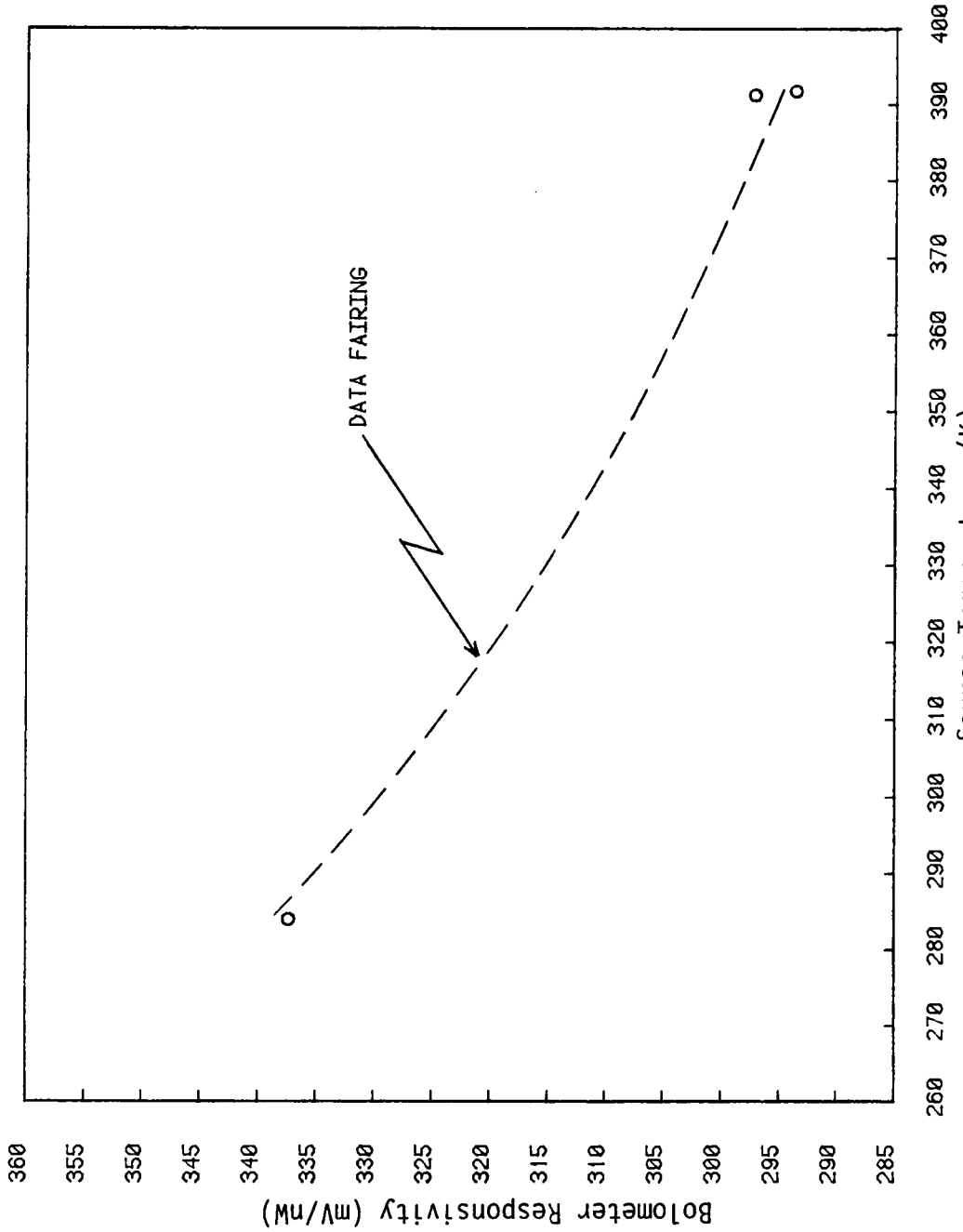
c. March 8 Responsivity

Figure 20. (continued)



d. March 9 Responsivity

Figure 20. (continued)



e. March 13 Responsivity

Figure 20. (continued)

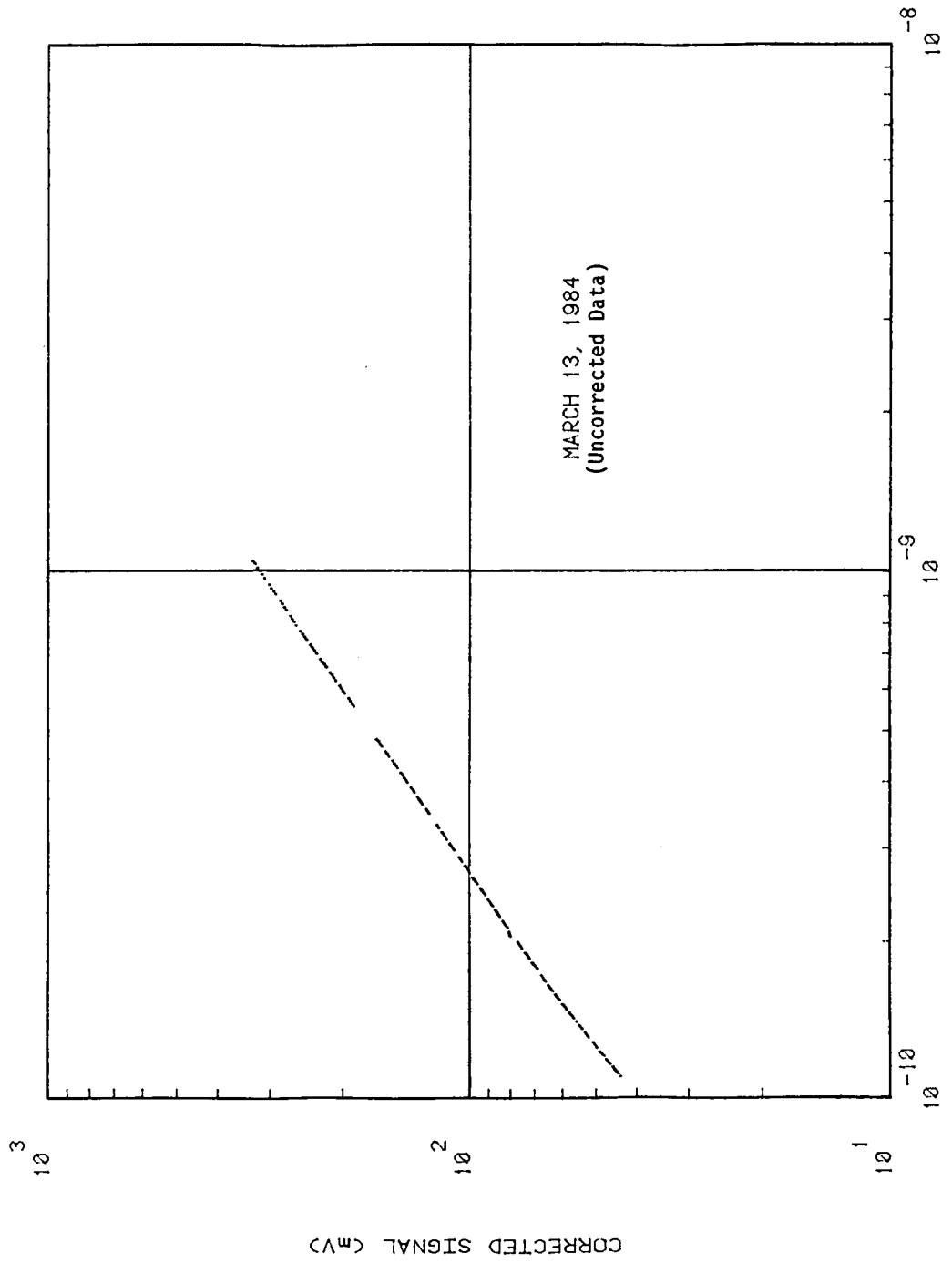


Figure 21. Dynamic Data, 50 Points per Sample.

Fifty-point samples, on the other hand, are a closely spaced continuum of events with minimal operator intervention. Arbitrarily selected numbers of the 50-point data set were fully corrected and used to compute responsivities found in Table 3. These points are plotted (Fig. 22) in the same format as the 500-point data of Figs. 20a through 20e. In Fig. 23, the concatenation of all data sets illustrates that 50- and 500-point samples describe the same bolometer performance. The best curve fit equation through the data is shown in Fig. 24.

Manual data points were taken on March 8, 9, and 12. When corrected according to Eqs. (1) through (5), the calculated responsivity merged flawlessly with the results found in Fig. 24. Although not included in this report, manually acquired data is mentioned because it confirms the accuracy of automated data acquisition; and because it demonstrates that the effects of computer-generated noise on the calibration were negligible, by achieving the same results with the 4052 terminal out of the loop.

B. Discussion of Results

The data in Figs. 20 through 24 show that the bolometer response was nonlinear. The shape of the curve initially indicated detector saturation, but incident power levels in the nano-watt range were unlikely to cause

Table 3. Dynamic Data Obtained on March 13, 1984 (50 points/sample)

Source Temperature (K)	Signal Data		Corrected Results		
	Source E_S (mV)	Tare E_T (mV)	Signal (mV)	Power (nW)	Responsivity (mV/nW)
391.75	276.00	53.28	330.64	1.11285	297.11
383.43	252.92	52.39	306.57	1.02128	300.19
370.61	219.50	51.17	271.79	0.89139	304.90
359.12	191.50	49.94	242.44	0.78589	308.49
348.51	168.04	48.73	217.67	0.69705	312.27
338.64	147.99	47.60	196.40	0.62138	316.07
319.78	114.11	45.41	160.18	0.49409	324.19
312.29	102.17	44.54	147.32	0.44940	327.81
300.45	85.05	43.11	128.69	0.38503	334.24
289.34	70.50	41.95	112.92	0.33113	340.97
282.34	62.20	41.14	103.77	0.30026	345.60
275.64	54.71	40.23	95.33	0.27275	349.52
269.28	48.12	39.35	87.83	0.24843	353.54

Helium dewar pressure = 20 torr constant; therefore, E_{IC} = 41.3 mV.

Frequency = 16.6 Hz constant.

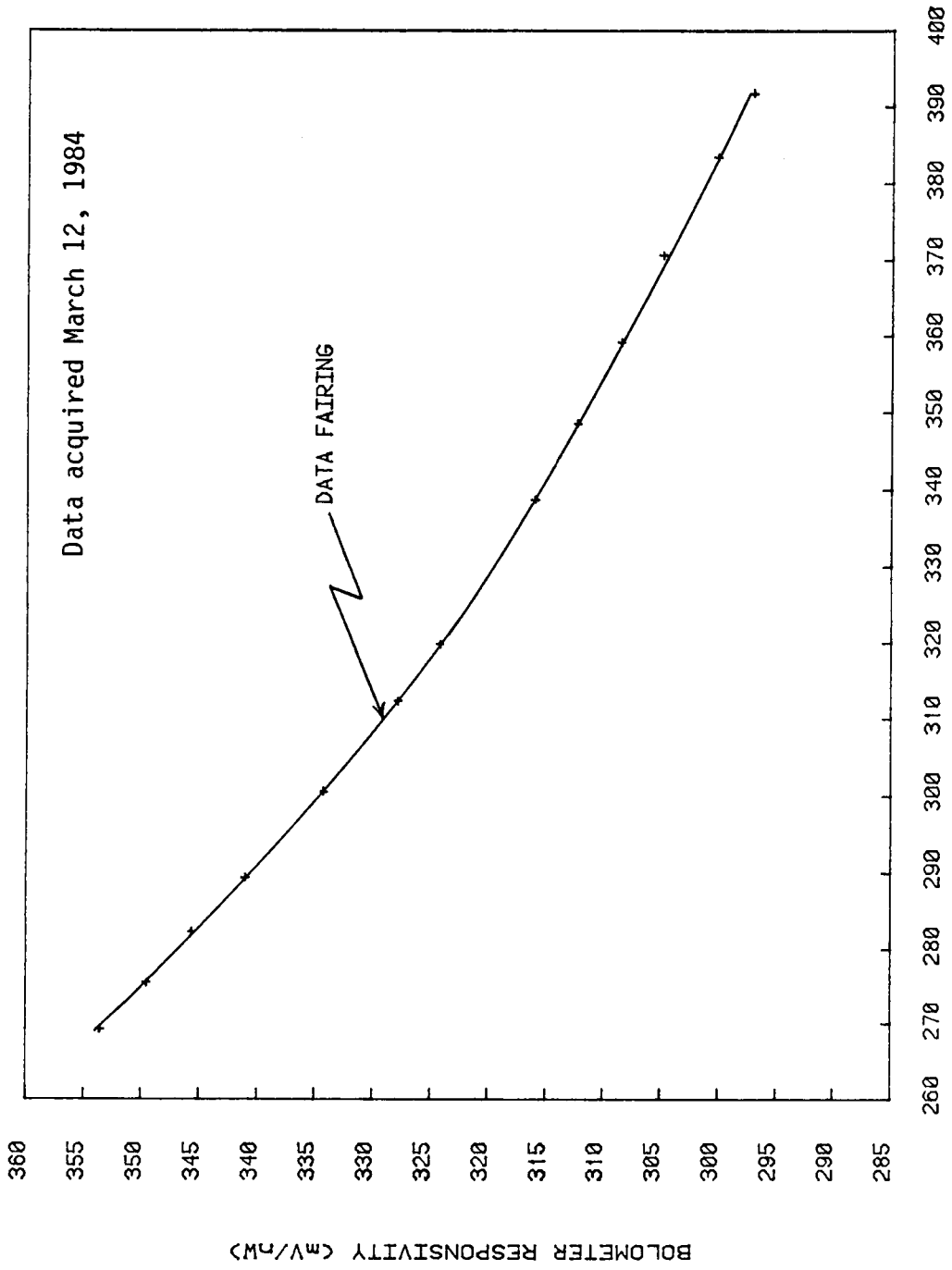


Figure 22. Dynamic Responsivity.

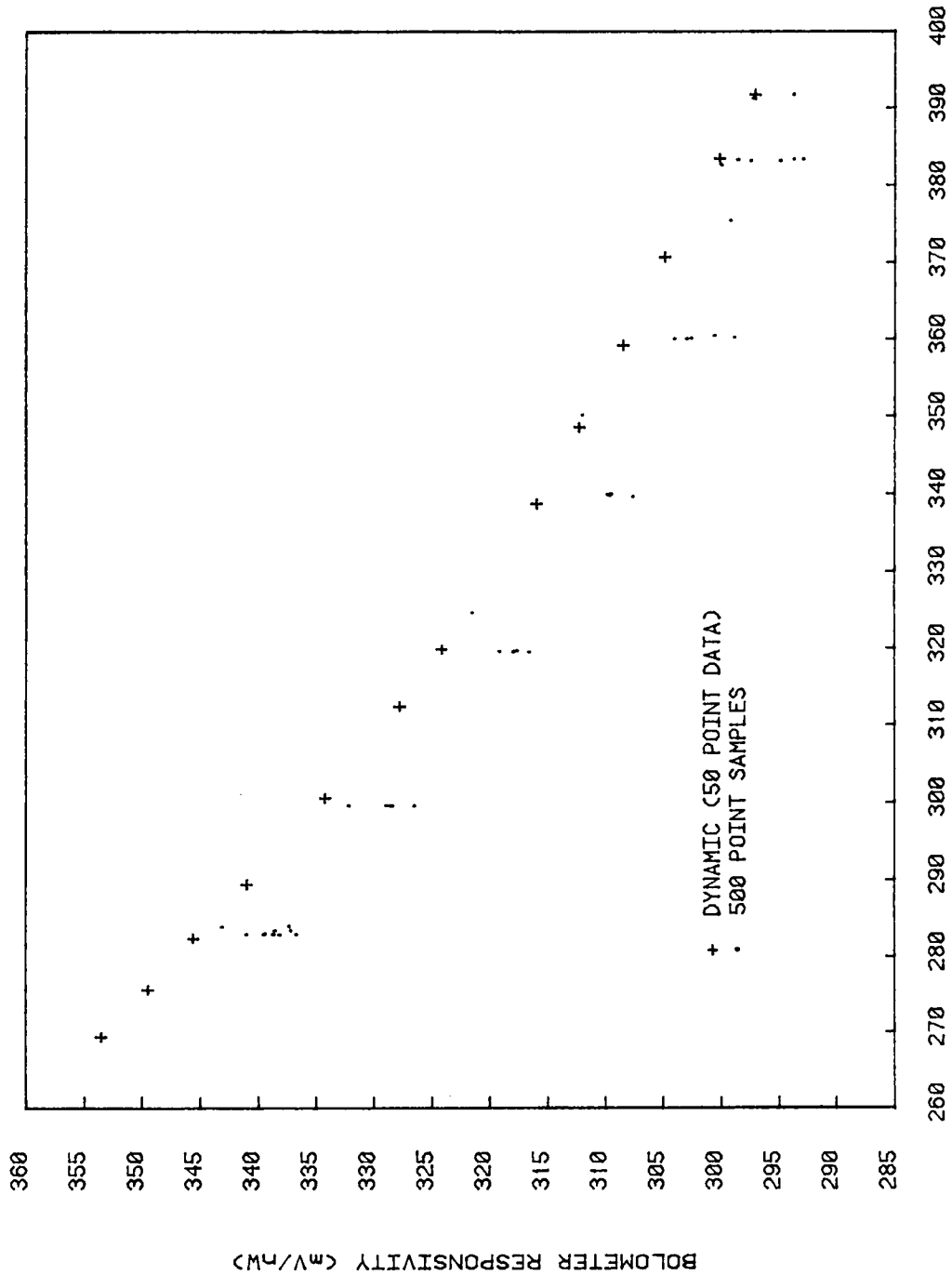


Figure 23. Inclusive Bolometer Responsivity Results.

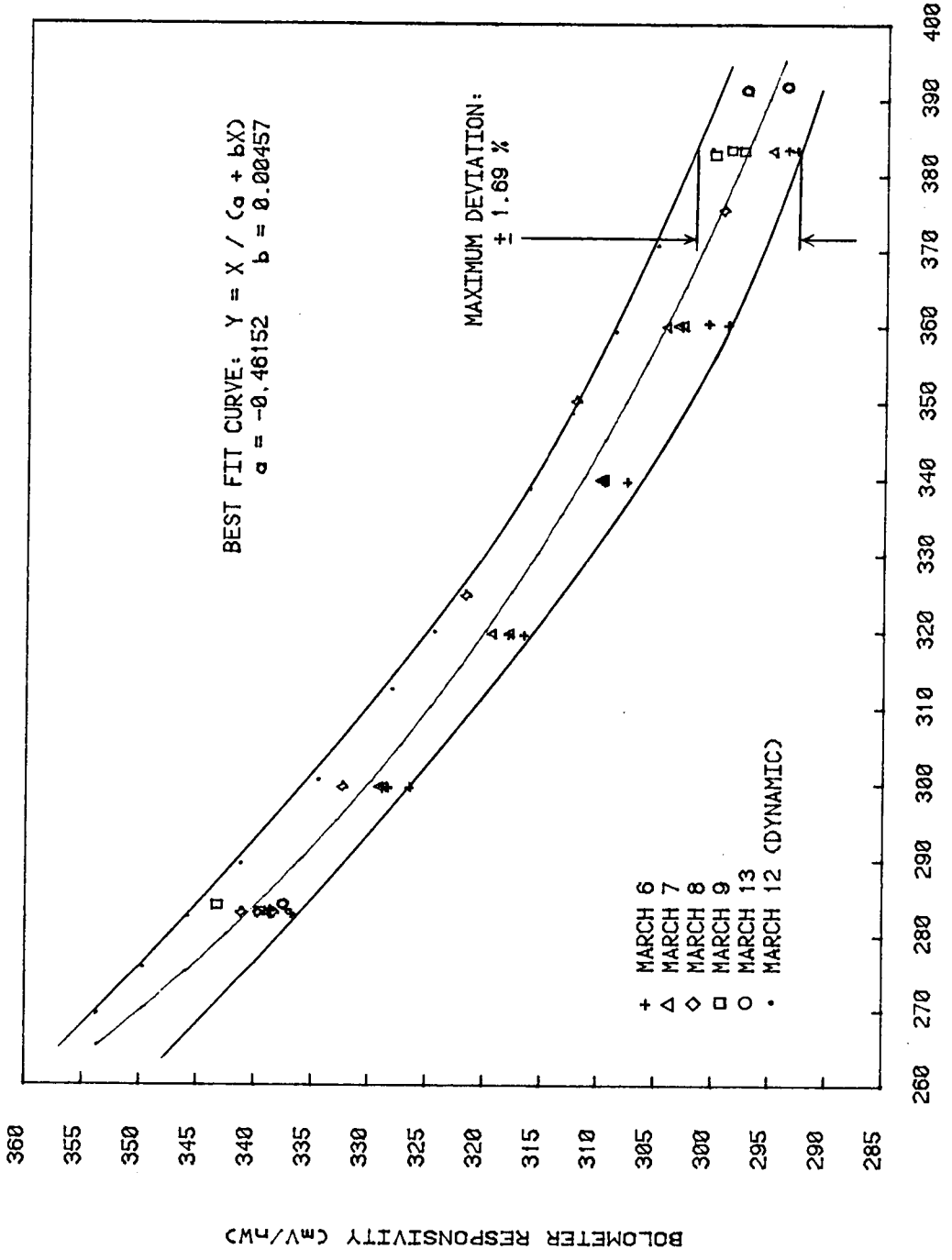


Figure 24. Responsivity Curve Fit and Scatter.

saturation. Close examination of the instrumentation and experimental methods did not reveal any other potential problems.

The calibration results were discussed with a representative of Infrared Laboratories [14], and his analysis indicted the load resistor. The detector and (7.6 MΩ) load resistor in series comprise the total circuit resistance, of which the bolometer element would ideally be about 1 percent. A more realistic goal would be 10 percent or less; however, with a cold resistance of 3.3 MΩ the detector element is in fact over 30 percent of the total resistance. The effect of this disproportion would be that a change in radiant power (i.e., source temperature) would change the bolometer (and hence the circuit) resistance. The resistance change would cause a variable bias and produce nonlinear response. Proof of this hypothesis will require cryogenic testing of the bolometer with a 30-MΩ (or greater) load resistor.

The Infrared Laboratories bolometer compares favorably with the Molectron bolometer [1] which is currently being used for calibration transfer. The new bolometer is handling fractional nano-watt power levels easily, which should enable direct handoff from the SIRS to the unisphere source in the future (Fig. 1, page 2). The mid-range responsivity of the Infrared Laboratories bolometer is

325×10^6 V/w, making it 480 times more sensitive than the Molectron (6.8×10^5 V/w) [1].

The most significant attribute of the new bolometer, however, is its repeatability. The data shown in Fig. 24 were acquired between March 6 and March 13, 1984. During that time the C^3 was twice cycled to near ambient temperatures and pressures in the millimeter range, which produced the effect of three separate pumpdowns. In addition, thermal cycling of the bolometer and the parametric variations of bias, chopping speed, and source temperature occurred on a daily basis. Notwithstanding these perturbations and the nonlinearity, the bolometer displayed excellent repeatability. The maximum deviation from the mean (at 383K) is $\pm$1.7 percent.

CHAPTER V

UNCERTAINTY

Uncertainty analysis of the calibration is divided into four sectors. The "known" beginning of this calibration is the SIRS which was calibrated by NBS. Reference [1] describes this process and assigns an uncertainty of 5 percent to the results.

Next, there are the various uncertainties associated with this calibration setup; distances, sizes, and instrumentation accuracy. These are analyzed in depth in Appendix C and summarized in Table 4.

Finally, there is data uncertainty which occurs on two levels. There is the scatter within 500-point samples; and the variation in responsivity at a single temperature, as a result of multiple 500-point sets. These can be referred to as short- and long-term precision.

Because of the complexities of data acquisition and the bolometer's nonlinear responsivity, it is difficult to reduce uncertainty to a single value. Calculations in this chapter will apply standard methods [15] and consider "worst case" possibilities. Following this conservative approach will lead to the use of high source temperature responsivity, where the deviation is the greatest.

Table 4. Experimental Uncertainty

Measurement	Uncertainty (%)
Bolometer Detector Area	±0.80
Ability to Measure Source Temperature	±0.37
Ability to Measure Internal Calibrator	±0.33
Source/Detector Separation Distance	±0.32
Ability to Measure Signal and Tare	±0.09
Total	±1.91

Equation (3) computes the signal using three sets of voltage readings. The short-term error contribution from each is expressed by Eqs. (7), (8), and (9):

$$U_S = \sigma_S/(E_S + E_T) \times 100 \ , \qquad (7)$$

$$U_T = \sigma_T/(E_S + E_T) \times 100 \ , \qquad (8)$$

$$U_{IC} = \sigma_{IC}/E_{IC} + 100 \ , \qquad (9)$$

where

U = response uncertainty (percentage),

σ = standard deviation of the sample,

E = signal voltage;

subscripts s, T, and IC stand for source, tare, and internal calibrator, respectively.

Table 5 shows the results when the above equations are applied to the six calibration runs made with the SIRS at 383K. Note that columns 2 and 3 are millivolt signals, while columns 4 through 6 are responsivity (10^6 V/w) or percentages thereof. A final mean and standard deviation accounts for the variation in column 6. Long-term drift, expressed by Eq. (10), is combined by the root-sum-squared (RSS) method with the factors in column 4, using Eq. (11).

$$U_d = (\sigma_d/\bar{R}_b) \times 100 = \pm 0.96\% \ , \qquad (10)$$

Table 5. Data Uncertainty

Run No.	Signal (mV)	Standard Deviation σ (mV)	Uncertainty (% of R_b)	RSS Uncertainty of Run (% of R_b)	Responsivity R_b (10^6 V/w)
1	E_S = 279.033	±0.4779	±0.1596		
	E_T = 17.955	±0.4164	±0.1390		
	E_{IC} = 40.956	±0.2561	±0.6253		
	E_b = 298.7834			±0.6602	292.892
2	E_S = 278.399	±0.4404	±0.1474		
	E_T = 17.955	±0.4164	±0.1393		
	E_{IC} = 40.957	±0.2561	±0.6253		
	E_b = 299.6714			±0.6574	293.702
3	E_S = 290.706	±0.0953	±0.0318		
	E_T = 10.505	±0.0526	±0.0175		
	E_{IC} = 41.499	±0.1693	±0.4080		
	E_b = 300.3514			±0.4096	294.860

Table 5. (continued)

Run No.	Signal (mV)	Standard Deviation σ (mV)	Uncertainty (% of R_b)	RSS Uncertainty of Run (% of R_b)	Responsivity R_b (10^6 V/w)
4	E_s = 291.028	±0.0789	±0.0259		
	E_T = 10.0571	±0.0720	±0.0236		
	E_{IC} = 40.8075	±0.1443	±0.3536		
	E_b = 303.7116			±0.3553	299.971
5	E_s = 292.023	±0.0719	±0.0236		
	E_T = 9.637	±0.0476	±0.0156		
	E_{IC} = 40.808	±0.1443	±0.3536		
	E_b = 304.2866			±0.3547	298.568
6	E_s = 284.500	±0.1157	±0.0381		
	E_T = 15.187	±0.0229	±0.0076		
	E_{IC} = 40.808	±0.1443	±0.3536		
	E_b = 302.844			±0.3557	297.432

$R_b = 296.2375 \times 10^6$ V/w

$\sigma_d = \pm 2.8396 \times 10^6$ V/w

$U_d = 0.96$ percent

where

σ_d = standard deviation of values in column 5,

$\bar{R}_b$ = mean value of responsivities from column 5,

U_d = long-term drift;

$$U_D = \left[\sum_{i=1}^{6} \left(U_{s_i}^2 + U_{T_i}^2 + U_{IC_i}^2 \right) + U_d^2 \right]^{1/2} . \qquad (11)$$

The total data uncertainty, U_D, yielded by Eq. (11) is U_D = 1.53 percent, which is equivalent to $\sigma_D = \pm 4.53 \times 10^6$ V/w.

All necessary factors have now been determined to calculate the uncertainty of the calibration. Experimental uncertainty (Table 4) and the SIRS uncertainty will be considered as residuals of previous calibrations and combined:

$$B = (5^2 + 1.91^2)^{1/2} = 5.35\% . \qquad (12)$$

The number of samples at this point is N = 6; thus, the Student's t-factor for 95-percent confidence is 2.477. Equation (13) provides the means of computing the final calibration uncertainty, assuming that the distribution of responsivity values is Gaussian:

$$R = \bar{R}_b \pm \frac{t_{\alpha/2}\ \sigma_D}{\sqrt{N}} \pm \bar{R}_b\ B . \qquad (13)$$

Substitution of the appropriate values from Eq. (13) yields $R = 296.24 \times 10^6 \pm 20.43 \times 10^6$ V/w, or an uncertainty for the entire calibration of ± 6.90 percent. Three observations should be made about this value. First, only the number for uncertainty is germane to this discussion since the response is nonlinear. Second, the most pessimistic location and assumptions make this a conservative estimate of uncertainty. Finally, the largest component of the final uncertainty is the 5-percent residual of the SIRS NBS calibration.

CHAPTER VI

FUTURE WORK

While the final calibration data were very good, a number of improvements are suggested for future work. These improvements will be directed toward the bolometer, reducing system noise, and enhanced data acquisition.

Bolometer improvements which have already been introduced will be briefly reiterated here. The ambiguous effect of detector bias mentioned in Chapter III, Section A, needs to be resolved. If the decision is made to replace the battery with a power supply, then the full load curve test should be performed to select the optimum bias current. Driving the internal calibrator with power supplies would also eliminate any doubt about battery drain altering the calibrator output. Once the internal calibrator has been isolated from power fluctuation, a large volume of IC data should be taken, varying only the helium pressure. It is possible that a direct signal correction can be made from dewar pressure, thus leaving the internal calibrator higher resolution to measure smaller variations in detector performance. A tuning fork chopper will eliminate the need for a frequency correction entirely and should greatly reduce the magnitude of the chopper tare through lower chopper operating temperatures.

The greatest single question to resolve about the bolometer is its nonlinear response. Cryogenic tests need to be performed with a 30-MΩ (or larger) resistor replacing the 7.6-MΩ load resistor. The new resistor must be mounted carefully to prevent vibration/capacitance-induced noise.

Replacement of the variable-speed chopper will have contributed to the reduction of system noise by eliminating fundamental and harmonic frequencies broadcast from the chopper controller. Data scatter caused by chopper instability should also be greatly reduced with the tuning fork chopper. A final major improvement in the noise regime would be to bring bolometer detector signals out of the chamber through a separate port, directly to the amplifier. During the work just completed, use of the standard C^3 wiring allowed the introduction of noise to the signal before amplification. The long leads also acted as antennas despite shielding and grounding.

Data acquisition can be improved by measuring the source, tare, and internal calibrator signals in closer time proximity. Since a finite time is required to block the SIRS, stop the chopper, stabilize the internal calibrator, and lock in on the signal, these measurements can never be made back to back. To the extent that they can be closer spaced, however, the readings are more likely to be describing the same operating state. It may be

sufficient to take a smaller number of data points per sample. A suggested acquisition scheme is shown in Table 6, where sample No. 5 begins the second cycle in the repeating pattern of 1 through 4. Chauvenet's criterion [16] will be applied to each sample, rejecting any points that would occur with a probability less than 1/2N (where N is the number of points per sample). If any points are rejected, replacements from the overflow region will be utilized to achieve the target sample size. The mean values of the two bracketing tare samples (2 and 4) will then be averaged to achieve the tare value associated with sample No. 3. Internal calibrator samples 1 and 5 will be handled in a similar manner to obtain the internal calibrator value.

Table 6. Data Acquisition Scheme

Sample No.	Type of Data	Points/ Sample	Overflow Points	Target Sample Size
1	Internal Calibrator	110	10	100
2	Tare	110	10	100
3	Source	550	50	500
4	Tare	110	10	100
5	Internal Calibrator	110	10	100

CHAPTER VII

CONCLUSIONS

The Infrared Laboratories bolometer suffered initially from reliability problems; however, these have now been overcome. The bolometer has excellent potential as a device for null calibration. A larger load resistor should eliminate the nonlinear response; however, even if this were not the case, nonlinearity would not interfere with the bolometer's effectiveness in a null calibration where repeatability is the crucial detector requirement. The data for this calibration were taken under a variety of conditions over a 13-day period and the near equivalent of three pumpdowns. Even so, detector repeatability was $\pm$1.2 percent, significantly better than any other detector tested thus far at AEDC. The new bolometer also has sensitivity that is 480 times greater than the Molectron bolometer, giving it the potential for direct calibration of attenuated sources such as the unisphere.

BIBLIOGRAPHY

BIBLIOGRAPHY

1. Sherrell, F. G. "Infrared Standards to Improve Chamber 7V Beam Irradiance Calibrations," Arnold Engineering Development Center TR-80-45, Arnold Air Force Station, Tennessee, January 1981.

2. Jarratt, K. B. "Development of Improved LWIR Source Calibration Techniques for Application to Sensor Testing at AEDC," Arnold Engineering Development Center TR-82-8, Arnold Air Force Station, Tennessee, July 1982.

3. Kunz, L. W. "An Improved Silicon Bolometer with Self-calibrating Capability," Society of Photo-Optical Instrumentation Engineers, 67:37-40, August 1975.

4. Sherrell, F. G. "Applications of a Self-calibrating Silicon Bolometer," Arnold Engineering Development Center TR-76-145, Arnold Air Force Station, Tennessee, October 1976.

5. Belew, P. W., and F. G. Sherrell. "Evaluation of a Self-calibrating Silicon Bolometer," Arnold Engineering Development Center TR-78-74, Arnold Air Force Station, Tennessee, April 1979.

6. Little, H. R., J. Hiatt, and K. A. Lienemann. "Low Temperature Infrared Source Calibration and Traceability at AEDC," Society of Photo-Optical Instrumentation Engineers, 416:136-144, April 1983.

7. Davidson, A. W. "Infrared Laboratories Bolometer Operating Manual," Infrared Laboratories, Inc., Tucson, Arizona, 1982.

8. Wyncke, B., et al. "The Effect of Temperature Fluctuations of Pumped Liquid Helium Bath on the Function of a Germanium Bolometer," Infrared Physics, 22(No. 5):313-315, September 1982.

9. Hiatt, Jay, and J. E. Shepherd. "Component Checkout Chamber (C^3)," Arnold Engineering Development Center TMR-82-V29, Arnold Air Force Station, Tennessee, October 1982.

10. El-Ataway, S., et al. "Evaluation of Composite Bolometers at 0.4 Kelvin," International Journal of Infrared and Millimeter Waves, 1(No. 3):110-114, May 1980.

11. Cryogenic Materials Data Handbook. TDR-64-280. Wright-Patterson Air Force Base, Ohio: Air Force Material Lab, 1970.

12. Fussell, W. B. Optical Radiation Measurements: Table of Diffraction Losses. (NBS Technical Note 594-8, Library of Congress 74-6000088.) National Bureau of Standards, United States Department of Commerce. Washington: Government Printing Office, 1984.

13. Yokley, C. R. Private communication. National Bureau of Standards, Washington, D.C., April 1984.

14. Robert Kurtz. Private communication. Infrared Laboratories, Tucson, Arizona, July 1984.

15. Abernathy, R. B., and J. W. Thompson. "Handbook--Uncertainty in Gas Turbine Measurements," Arnold Engineering Development Center TR-73-5, Arnold Air Force Station, Tennessee, January 1973.

16. Holman, J. P. Experimental Methods for Engineers. New York: McGraw-Hill, 1978.

APPENDIXES

APPENDIX A

NOISE MEASUREMENTS

The bolometer was tested for noise during January 1983, in its ambient configuration. The objectives of this test were: (1) to measure noise and calculate the minimum detectable signal, (2) to evaluate measured noise relative to theoretical calculations, and (3) to compare noise levels with data provided by the bolometer manufacturer.

Figure A-1 illustrates a simplified circuit diagram of the bolometer; "A1" is the cooled first-stage pre-amp, and "A2" represents the combination of the OP-27 and OP-12 amplifiers (Fig. 4, page 8). Gain and input noise specifications of the amplifier elements are found in Table A-1. The load resistor value is R_L = 7.6 MΩ, and when cooled to 1.94K the bolometer resistance is R_B = 3.3 MΩ. With the bias removed and R_L shorted to ground, the FET input resistance becomes R_L parallel with R_B (Eq. (A-1)), or R_{FET} = 2.3 MΩ:

$$R_{FET} = \frac{R_L R_B}{R_L + R_B} . \qquad \text{(A-1)}$$

The Johnson noise of the detector was calculated (Eq. (A-2)) to be 1.57 x 10^{-8} V/$\sqrt{Hz}$:

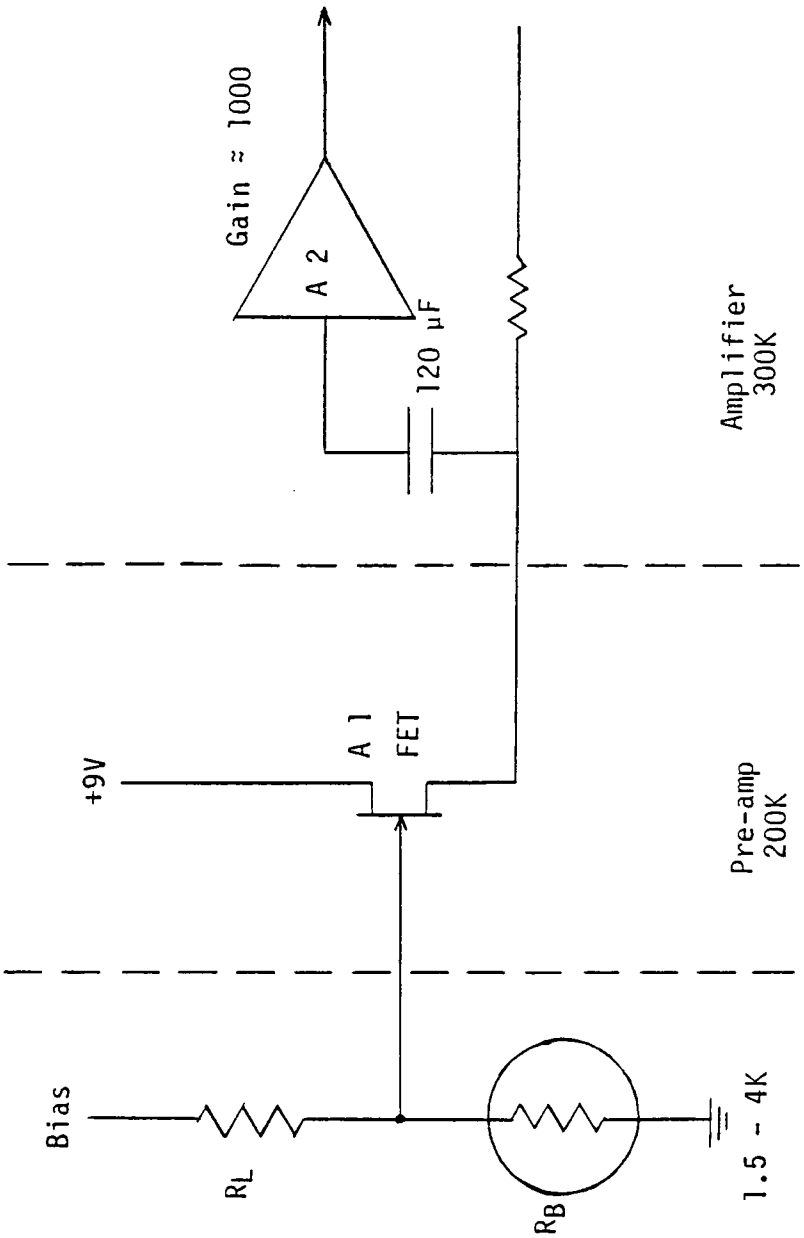


Figure A-1. Bolometer/Amplifier Simplified Circuit.

Table A-1. Amplifier Specifications

Component	Operating Temperature	Gain	*Input Noise Voltage Density
J-230 FET	200K	0.95	8×10^{-9} V/$\sqrt{\text{Hz}}$
OP-27	300K	100	3.5×10^{-9} V/$\sqrt{\text{Hz}}$
OP-12	300K	9.1	2.2×10^{-8} V/$\sqrt{\text{Hz}}$

*At 10 Hz.

$$N_J = [4\ K\ T_B\ B_F\ R_{FET}]^{1/2}\ , \qquad \text{(A-2)}$$

where

K = Boltzmann's constant = 1.3807×10^{-23} joule/K,

T_B = absolute operating temperature of bolometer = 1.94K,

B_F = frequency bandwidth = 1 Hz,

R_{FET} = FET input resistance defined by Eq. (A-1).

Amplifier noise values from Table A-1 were combined with Johnson noise using Eq. (A-3) to obtain the total calculated noise of the bolometer system:

$$N_T = [(N_{FET})^2 + (N_{OP-27})^2 + (N_{OP-12})^2 + (N_J)^2]^{1/2}\ . \qquad \text{(A-3)}$$

The result was $N_T = 2.84 \times 10^{-8}\ V/\sqrt{Hz}$.

Bolometer noise was then measured using the spectrum analyzer from 0 to 25 Hz (Fig. A-2), with a 150-mHz window. Noise was measured at two conditions: with normal bias and with zero bias on the detector. The values at 10 Hz were -86 and -96 dBV, respectively. Decibels were then converted to signals, using Eq. (A-4):

$$V_N = \frac{2.582 \times 10^{\text{dBV}/20}}{1000}\ , \qquad \text{(A-4)}$$

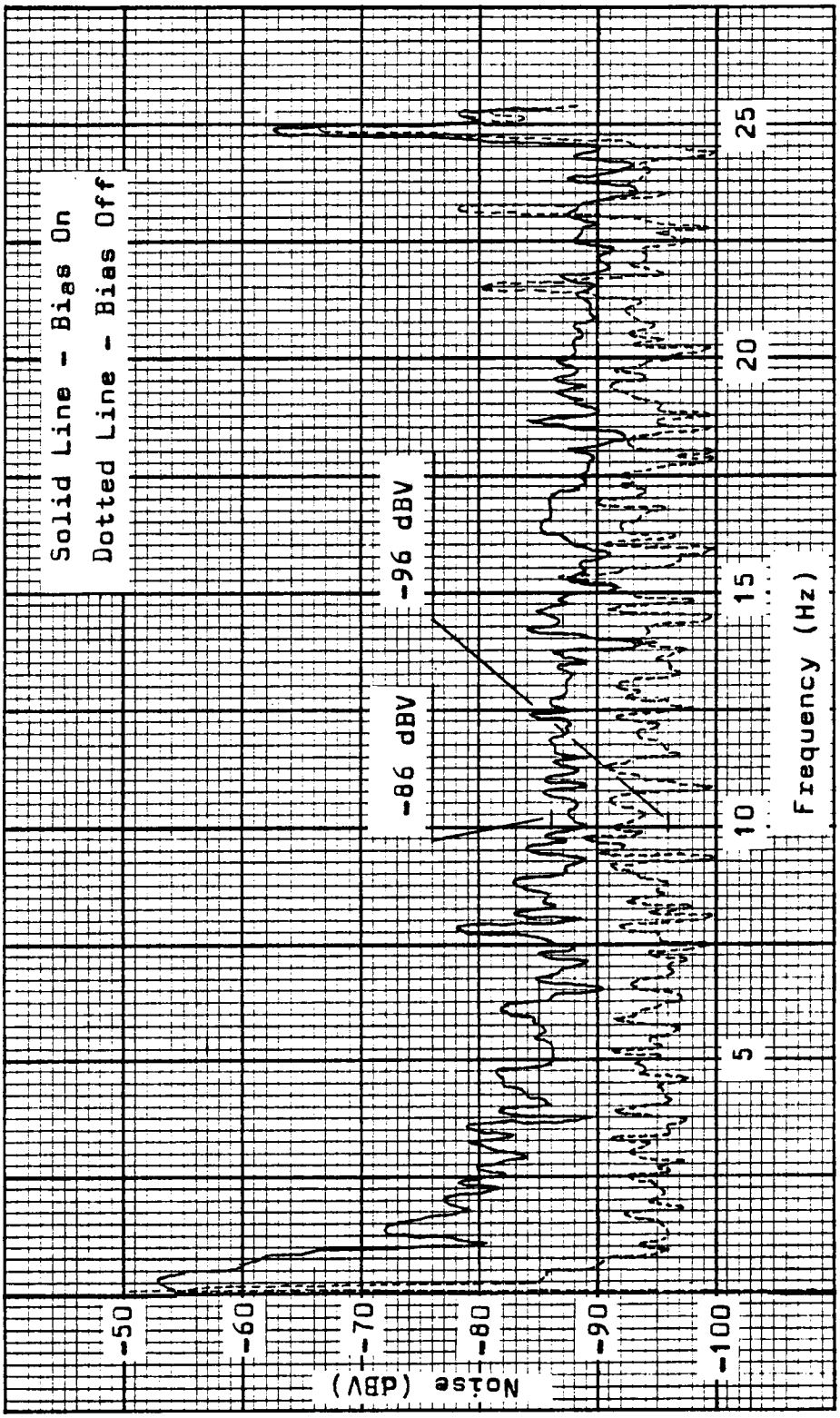


Figure A-2. Bolometer Noise Spectrum.

where

V_N = equivalent noise signal,

2.582 = normalizing factor from 150 mHz to 1 Hz,

dBV = decibel noise level,

1000 = conversion of millivolts to volts.

Total noise was 1.294×10^{-7} V/$\sqrt{\text{Hz}}$ with bias, and 4.092×10^{-8} V/$\sqrt{\text{Hz}}$ without bias. The other notable fact in Fig. A-2 was the low 1/f knee at 5 Hz.

Infrared Laboratories provided noise data taken at 20 Hz. Their measurements were 5.85×10^{-8} V/$\sqrt{\text{Hz}}$ with 0.9 μA bias, and 5.2×10^{-9} V/$\sqrt{\text{Hz}}$ with zero bias. Infrared Laboratories data were obtained by inserting various resistors, filters, and bias batteries into the test circuit, a method far more complex than the use of the spectrum analyzer. The fact that manufacturer's data were taken at 20 Hz rather than 10 Hz has a negligible effect on the noise measurements.

The calculated noise and noise measurements show that the lower limit of the detector will be set by Johnson noise while amplifier noise is insignificant. The increase in noise level with bias on is primarily from the bolometer looking at the 300K window. There is excellent correlation between noise measurements, calculations, and manufacturer's data. All three fall easily within an order of magnitude at zero bias conditions. The noise floor of

1.29×10^{-7} $V/\sqrt{Hz}$ with detector bias implies that microvolt signal levels could be measured by the bolometer with a signal/noise ratio of 10. Test-peculiar noise under experimental conditions, however, is more likely to limit the detector's ability to measure small signals than Johnson noise or amplifier noise. It appears that the cooled FET pre-amp has produced significant improvement over the MOSFET used by the Molectron bolometer, which had 1/f corner frequency of 25 Hz.

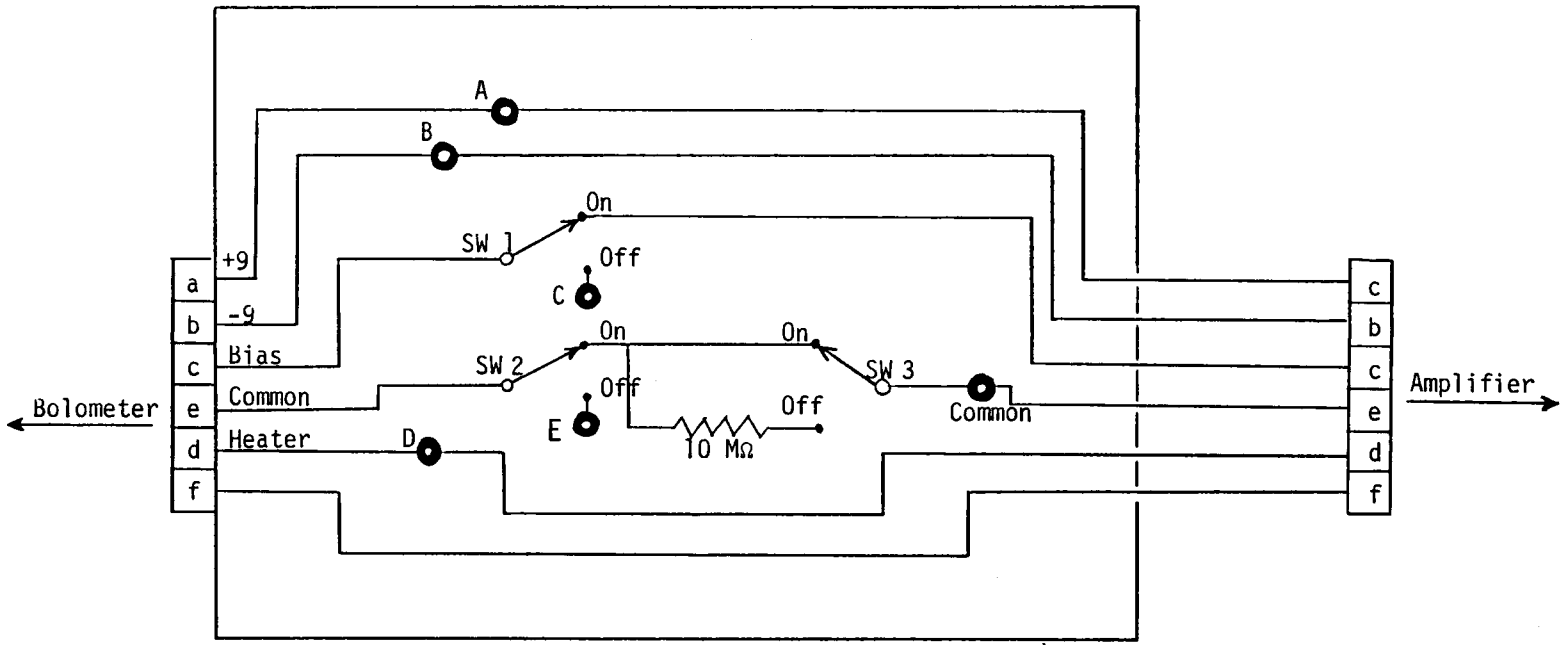
Noise conditions were evaluated again in March 1984, when the bolometer was installed in the C^3 for calibration. The bolometer was in its cryogenic configuration at this time, and a number of noise sources were present that had not been involved in the earlier noise measurements. In addition, several changes had been made to the bolometer/amplifier circuit, including much longer signal leads.

Noise sources identified were: an unshielded IEEE-488 cable connecting the Tektronix® 4052 to the EG&G 5206 lock-in amplifier; the C^3 internal ion gage; and 60-cycle pickup. Long signal leads, insufficient grounding, and the proximity of the bolometer amplifier to the chopper control unit also contributed to the noise. At one point, low-frequency (less than 3 Hz) mechanical vibration from the 4-KW cooling plant was observed, and inevitably, noise spikes from the lab/shop environment were randomly present.

The most significant change in the bolometer circuit was the physical separation of the amplifier from the bolometer by 30 ft of connecting cables. Next, the FET heater lead was brought out separately, and a diagnostic circuit (Fig. A-3) was inserted to allow the electrical isolation of individual bolometer/pre-amp components.

The IEEE-488 cable was replaced with a shielded cable and rerouted. The ion gage was turned off, and instrument power plugs were rearranged to reduce noise on the bolometer circuit. The addition of heavier grounding wires provided significant reduction in 60-Hz pickup. Nothing could be done at the time about the length of signal lines or random environmental noise. The problem with chopper controller broadcast was not observed until calibration had begun. Problems with the 4-KW plant noise were circumvented by not taking data while the plant was operating.

Figures A-4 through A-8 record the bolometer noise under various operating conditions as displayed by the spectrum analyzer. Figure A-4 shows the spectrum analyzer output with zero bias. The noise floor was nearly an order of magnitude higher than in earlier tests (78.3 dBV or 3.14×10^{-7} V/$\sqrt{\text{Hz}}$); however, the 1/f corner was still less than 5 Hz. Figure A-5 is the noise spectrum with bias on. The source of the spike at 9.3 Hz was unknown,



Normal Operation

1) Switch 1 on
2) Switch 2 on
3) Switch 3 on

Amplifier Checkout

1) Switch 1 on
2) Switch 2 on
3) Switch 3 off
4) Read Signal at B, Common

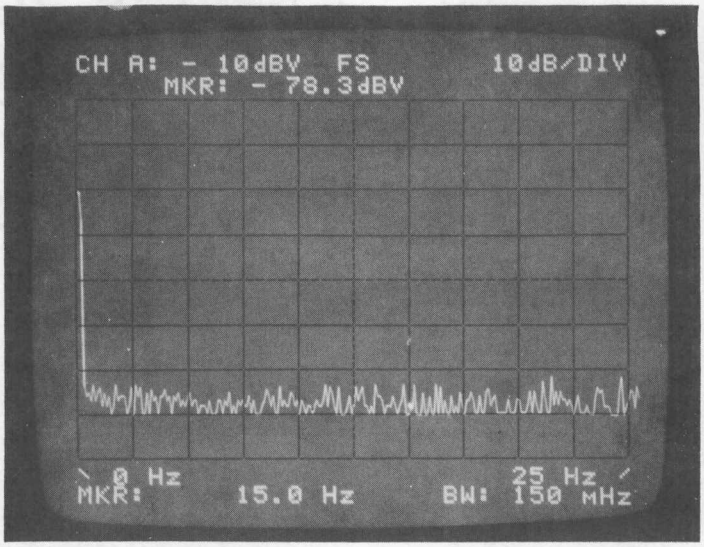
Bolometer Resistance

1) Switch 1 off
2) Switch 2 off
3) Read resistance at C,E

Resistance Heater

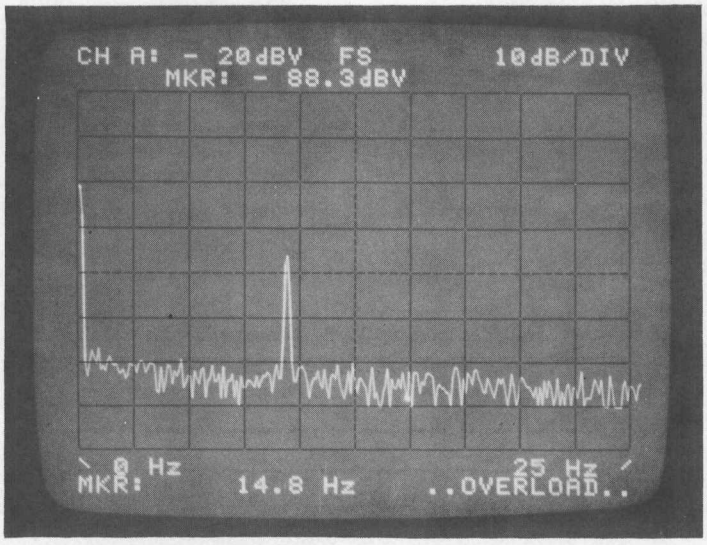
1) Switch 2 off
2) Read Resistance at A,D

Figure A-3. Bolometer Diagnostic Circuit.



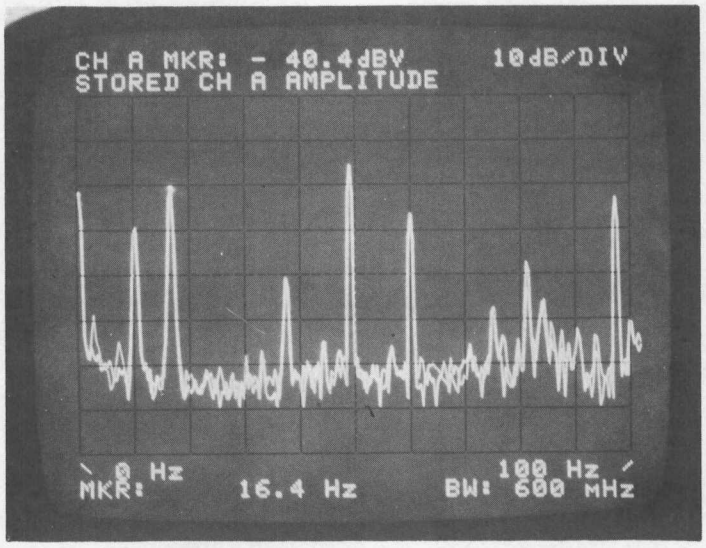
No Source,
20K Background

Figure A-4. Zero Bias Noise Spectrum.



No Source,
20K Background

Figure A-5. Normal Bias Noise Spectrum.



Shutter Blocking, Chopper at 16.4 Hz

Figure A-6. Noise Spectrum with Chopper Harmonics.

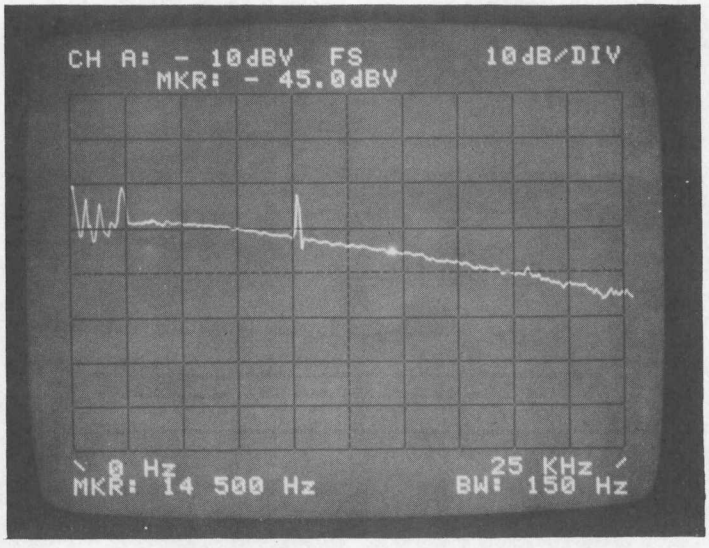
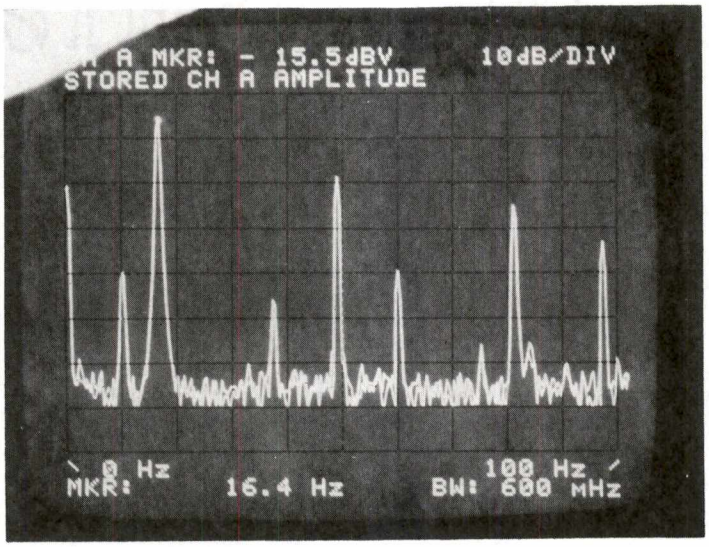


Figure A-7. Noise Spectrum: Communications Surge.



Blackbody Source at 340 Kelvin

Figure A-8. Noise Spectrum: Comparison with/without Tektronix® Active.

but closely resembled a 7.9-Hz vibration component found on the Molectron bolometer under similar conditions. Again, noise levels were slightly higher than before (88.3 dBV or 9.93×10^{-8} V/$\sqrt{\text{Hz}}$). Figure A-6 illustrates the problem with chopper pickup. The spike at 49.2 Hz (third harmonic of 16.4 Hz) is larger than the fundamental.

Communication between the Tektronix® and the scanner occasionally produced surges such as the one seen in Fig. A-7, which caused much initial consternation; however, analysis of the data acquisition sequence proved that the effects on data were negligible. The surge is prompted by the "initialization" command to the scanner. This command is followed by a series of pressure/temperature readings via the Fluke voltmeter, during which the surge dies down. Bolometer signals are then read by direct communication between the Tektronix® and the EG&G 5206 lock-in amplifier. This data link causes no noise problems, as evidenced by Fig. A-8. This figure shows a dual trace of the noise spectrum with and without the Tektronix®-EG&G communicating. The two traces are almost indistinguishable.

There was a secondary level of insidious communication between the lock-in and the spectrum analyzer. The overload light on the spectrum analyzer flashed synchronously with the talk/listen light on the lock-in amplifier as it was queried by the Tektronix®. The overload

condition had an adverse impact on the spectrum analyzer's ability to measure noise basement levels while calibration data were being acquired. The sensitivity of the spectrum analyzer had to be reduced to avoid the overload, which had the concurrent effect of decreasing its ability to measure small signals.

Nothing in the spectrum or the measured bolometer signals indicated that voltage levels were being affected by the illicit communication; however, electromagnetic compatibility between the digital equipment and the analog circuitry cannot be ignored. Since the FET output signals can be utilized in the nanovolt range, EMI coupling must be reduced as much as possible. This may be accomplished by implementing the following changes:

1. Move the bolometer amplifier as close as possible to the chamber.
2. Separate the bolometer cables from all other cables.
3. Reduce line coupling from power supplies.

APPENDIX B

DIMENSIONAL PARAMETERS AND CORRECTIONS

This appendix consists of measurements, sensor calibrations, and calculations made prior to, and in support of, the actual bolometer calibration. Section 1 includes physical measurements including shrinkage corrections at 20K. Section 2 covers temperature sensor calibrations.

1. Physical Measurements and Corrections

The spacing and size of elements inside the bolometer were measured at the precision measurement lab on December 9, 1983, under supervision of the project engineer. No formal report was made. The bolometer was in its chamber test configuration with the KRS-5 window and vacuum jacket bottom removed. The bolometer flexure ensured rigid (and correct) alignment. Figure B-1 labels the various points. The outer surface of the window flange (H) was firmly clamped to the measurement table and used as the reference surface. Measurements are recorded in Table B-1. The distance C-H (3.769 in. or 9.573 cm) is the internal distance from the reference flange to the detector at room temperature. The bolometer field of view is limited by the cold field stop at G to 3.897 deg (0.002 sr).

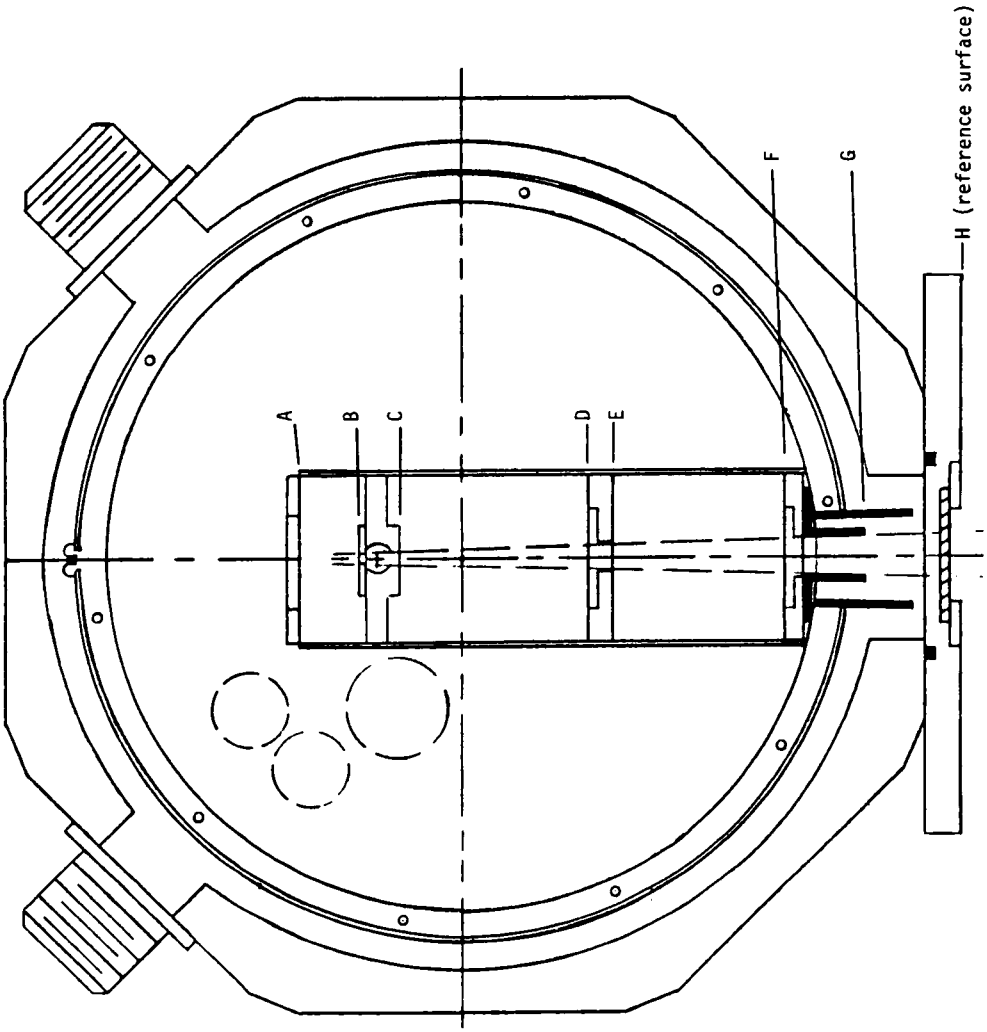


Figure B-1. Bolometer Internal Measurements Points.

Table B-1. Bolometer Internal Measurements

Location	Type Measurement	Dimension	
		English (in.)	Metric (cm)
A-H	Distance	4.624	11.745
B-H	Distance	4.028	10.231
C-H	Distance	3.769	9.573
D-H	Distance	2.648	6.725
E-H	Distance	2.527	6.419
F-H	Distance	1.409	3.578
G-H	Distance	0.818	2.078
H	Diameter	1.000	2.54
G	Diameter	0.250	0.635
E	Diameter	0.1875	0.476
D	Diameter	0.750	1.905
C*	Diameter	0.0492	0.125
B*	Diameter	0.0197	0.050
A-B**	Distance	0.5960	1.514
B-C**	Distance	0.2590	0.658
C-D**	Distance	1.1212	2.848
C-E**	Distance	1.2420	3.155
C-G**	Distance	2.9510	7.496
D-E**	Distance	0.1208	0.307
E-F**	Distance	1.1182	2.840
F-G**	Distance	0.5908	1.500

*Not measured--manufacturer's specifications.

**Indicates a calculated, rather than a measured distance.

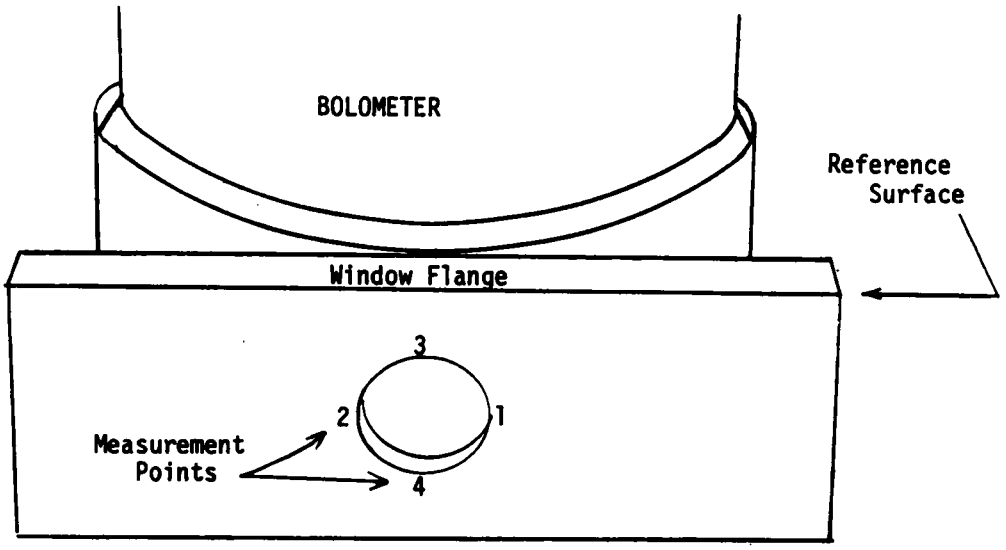
From Infrared Laboratories specifications:

Location	Diameter (mm)	Area (mm^2)
Bolometer Integrating Sphere	3.10	30.1907
Front Opening	1.25	1.2815
Rear Opening	0.5	0.1976

The ratio of aperture areas to total bolometer integrating sphere areas is 0.049. It is important that this figure be less than 0.05 to ensure blackness.

The *in situ* distance from the source test fixture to the source pinhole aperture was 1.477 in. The distance separating the reference faces of the source fixture and the bolometer was measured at four points around the perimeter of the window (Fig. B-2), before and after the chamber calibration. The arithmetic mean value 5.1969 in. (13.1976 cm) was used for calculations. Total source-detector separation was:

Source to Fixture	1.477
Fixture to Bolometer Flange	5.1969
Flange to Detector	3.769
Total	10.4429 in. (26.5250 cm)



Before Calibration 2/27/84
No. 1 Obstructed, not measured
No. 2 5.1955 in.
No. 3 5.1905 in.
No. 4 5.2029 in.

After Calibration 3/16/84
No. 1 5.1930 in.
No. 2 5.1975 in.
No. 3 5.1980 in.
No. 4 5.2012 in.

$\bar{X}$ = 5.1969 ±0.00489

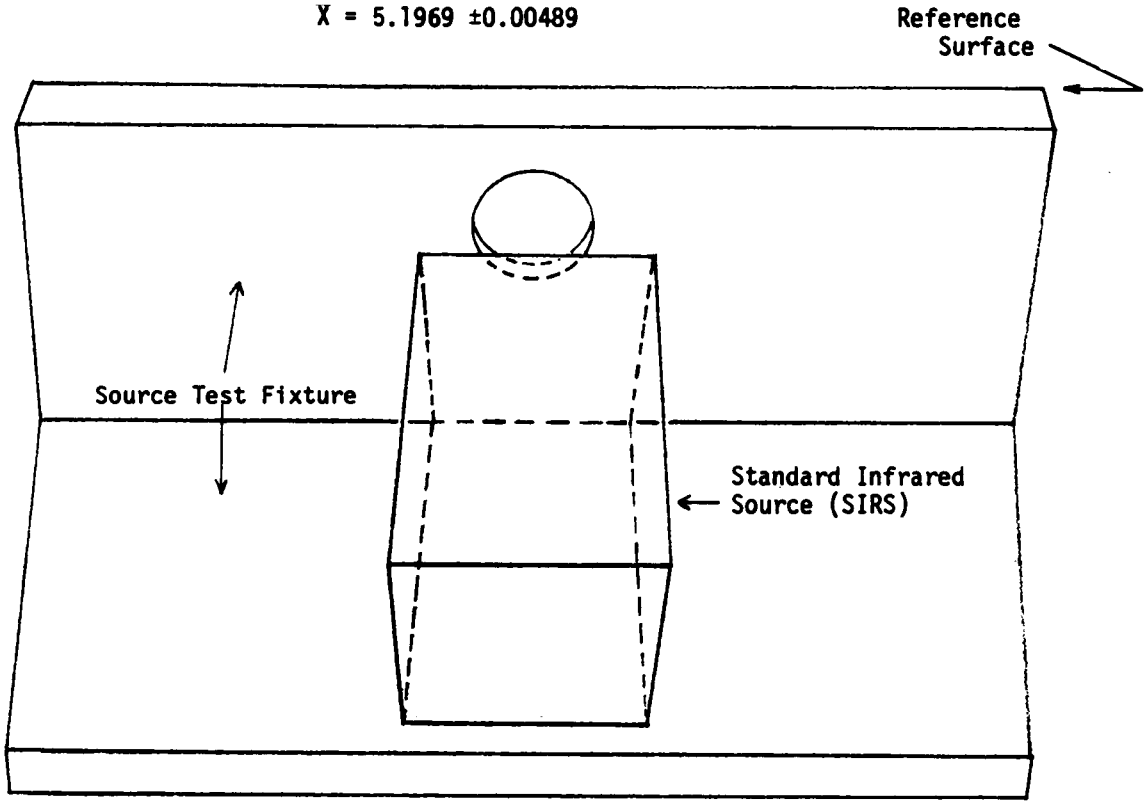


Figure B-2. Bolometer-Source Fixture Separation.

The source aperture was a copper/nickel Buckbee-Mears precision pinhole which had previously been measured as 0.02557 in.-diam. The shrinkage at 20K is 0.00326 in./in.; therefore,

$$0.0256 - (0.0256 \times 0.00326) = 0.02551634 \text{ in. } (0.0648 \text{ cm})$$

$$\text{Area of Source} = \pi\ (0.0324)^2 = 0.003299 \text{ cm}^2 .$$

Since all energy which enters the bolometer integrating cavity is eventually absorbed by the detector element, the admitting aperture is used as the detector area. The 0.125-cm pinhole is of copper and has a shrinkage of 0.00326 cm/cm at 1.95K; therefore,

$$0.125 - (0.125 \times 0.00326) = 0.12456 \text{ cm}$$

$$\text{Area of Detector} = \pi\ (0.0623)^2 = 0.01219 \text{ cm}^2 .$$

The source fixture and bolometer mounting fixture are both fixed to the C^3 20K cold plate, and all components are aluminum. The total separation at room temperature is 26.5224 cm, and the 20K shrinkage factor for aluminum is 0.00415 cm/cm; thus,

$$26.5224 - (26.5224 \times 0.00415) = 26.4124 \text{ cm} .$$

The bolometer detector element was overcoated with Nextel® Black Velvet paint. Figure B-3 shows the spectral absorptivity of this paint measured during previous work at AEDC. There are slight dips at 9 μm, but the paint is

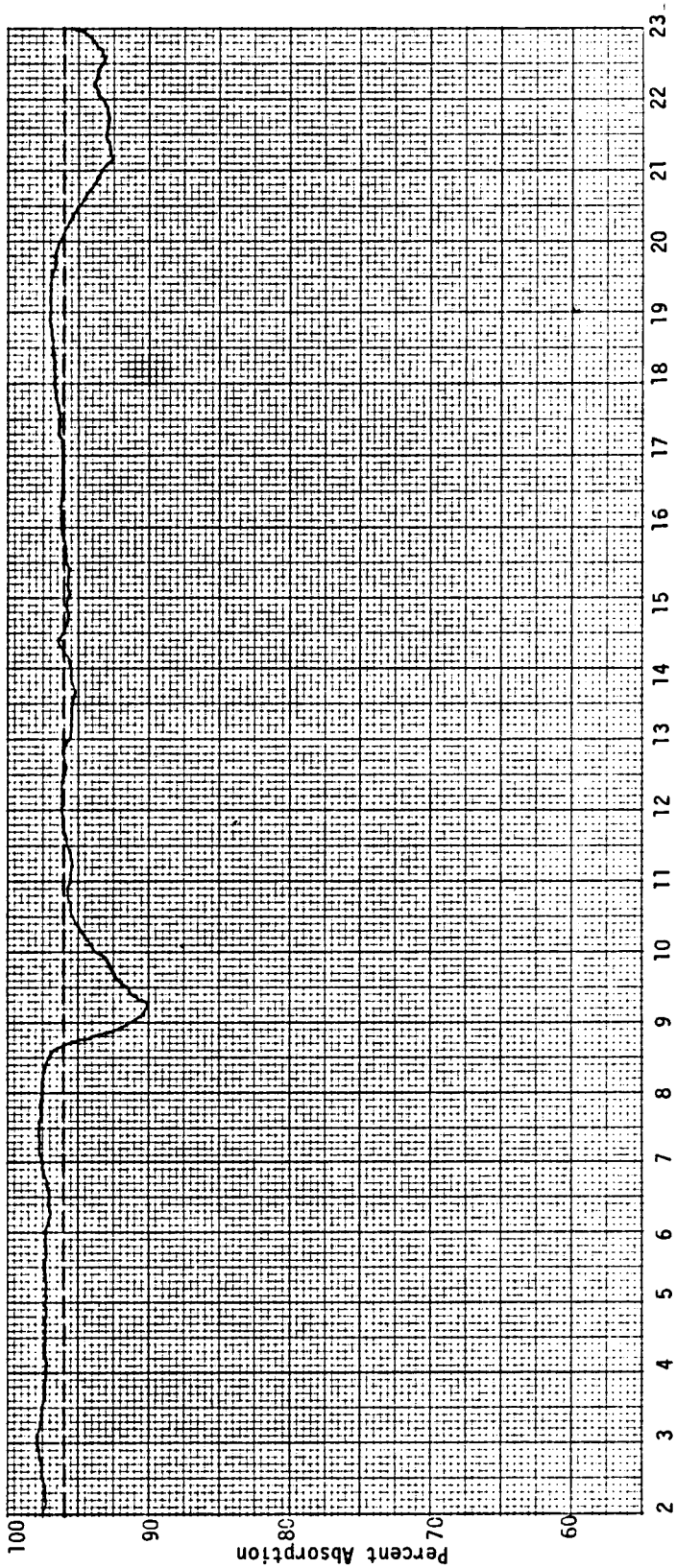


Figure B-3. Spectral Absorptivity of Nextel© Black Velvet Paint.

essentially black and absorbs 96 percent of incident energy in the range from 2 to 23 μm.

2. Temperature Sensor Calibrations

The SIRS blackbody has two precision thermistors imbedded in the core. Calibration of these sensors was performed before the blackbody was assembled, and Eqs. (B-1) and (B-2) were derived to calculate the thermometric temperature from sensors 1 and 2, respectively:

$$\frac{1{,}000}{T} = 2.37427 + 2.79430 \times 10^{-1} (\ell n\ e_T) - 2.37121 \times 10^{-2} (\ell n\ e_T)^2 + 6.14412 \times 10^{-3} (\ell n\ e_T)^3 - 4.86219 \times 10^{-4} (\ell n\ e_T)^4 \ ; \quad \text{(B-1)}$$

$$\frac{1{,}000}{T} = 2.34306 + 2.51712 \times 10^{-1} (\ell n\ e_T) - 4.94094 \times 10^{-3} (\ell n\ e_T)^2 + 1.54903 \times 10^{-3} (\ell n\ e_T)^3 - 1.10585 \times 10^{-4} (\ell n\ e_T)^4 \ . \quad \text{(B-2)}$$

Equation (B-3) was provided as a result of the NBS calibration of the SIRS. This equation corrects the temperatures produced by Eqs. (B-1) and (B-2) from thermometric temperatures to the absolute radiometric temperature of the blackbody:

$$T_R = -1.43799 + 1.00337\ T \ . \quad \text{(B-3)}$$

The bolometer operating temperature was determined primarily from the helium vapor pressure in the bolometer dewar. Pressure measurements were made with an MKS Baratron which was plumbed into the pumping line. This device had a 20-mm offset, which was corrected in the computer software. Pressure readings were converted into temperatures, using the standard NBS helium vapor pressure data in Table B-2.

Temperature sensors were mounted in numerous other locations: the chamber liner (three), the source fixture (two), the shutter, the SIRS housing, the cryogenic lines (two), and on the bolometer cold finger. These sensors provided a critical service in verification and diagnostics; however, since the bolometer calibration did not utilize their output directly, their calibrations will not be detailed.

A method was developed, using the OHAUS Model 1119 balance beam scale, to determine how much liquid helium was in the bolometer dewar. For the purpose of this discussion, the bolometer is considered to be in the ambient configuration including electrical units, the KRS-5 window, the nitrogen dewar cap, and the helium vapor pumping attachment. Volumes of the nitrogen and helium dewars were determined by filling them individually with freon and then pouring the contents into a graduated beaker.

Table B-2. Helium Vapor Pressure/Temperature

mm (Hg)	K
3.6335	1.5
5.7406	1.6
8.6612	1.7
12.5614	1.8
17.601	1.9
23.9199	2
31.6106	2.1
40.6754	2.2
51.2531	2.3
63.5739	2.4
77.7884	2.5
94.0407	2.6
112.474	2.7
133.227	2.8
156.437	2.9
182.242	3
210.782	3.1
242.192	3.2
276.61	3.3
314.174	3.4
355.03	3.5
399.334	3.6
447.258	3.7
498.988	3.8
554.723	3.9
614.68	4
679.152	4.1
748.459	4.2
822.418	4.3
901.013	4.4
984.366	4.5
1072.6	4.6

The nitrogen dewar volume was 850 ml and the helium dewar volume was 1,225 ml. Densities of the two cryogen liquids are 0.808 and 0.13 g/ml, respectively; therefore, the weight increase would be 688.2 grams of LN_2 and 157.2 grams of helium. Since the bolometer's empty weight as determined by the scale was 8.3175 Kg, with full dewars the weight would be 9.1629 Kg.

APPENDIX C

UNCERTAINTY

This appendix contains the calibrations, measurements, and calculations which are the basis for uncertainty analysis of the total calibration. Fundamental to this are Eqs. (C-1) through (C-4) which define responsivity:

$$\text{Signal } (S) = (E_s + E_T)\,\frac{41.3}{E_{IC}}\,, \qquad \text{(C-1)}$$

$$\text{Power } (P) = \frac{\alpha\varepsilon\sigma T^4 A_s(\pi r_b^2)}{2.22\ \pi D^2}\,, \qquad \text{(C-2)}$$

$$\text{Responsivity } (R_b) = \frac{\text{Signal}}{\text{Power}} = \frac{2.22\ \pi D^2 (E_s+E_T)\frac{41.3}{E_{IC}}}{\varepsilon\alpha\sigma T^4\ A_s\ \pi r_b^2}\,. \qquad \text{(C-3)}$$

Simplified,

$$R_b = \frac{C\ D^2\ (E_b)}{E_{IC} T^4\ A_s\ r_b^2}\,, \qquad \text{(C-4)}$$

where C is a constant, $E_b = E_s + E_T$, and r_b is the radius of the bolometer integrating cavity aperture.

The potential error of each factor in Eq. (C-4) must first be obtained. For voltages, this involves comparing the measuring device against a known input. The Fluke voltmeter reads signals from two sensors which were then used to compute the source temperature (T). An Analogic Voltage Standard, an AEDC secondary standard,

with calibration good through November 1984 was used as the input. Calibration data are shown in Table C-1.

Bolometer signals were read by the EG&G 5206 lock-in amplifier. The source of known A/C signal was the calibrated output of a PAR-124 lock-in amplifier. Results are shown in Table C-2.

Next, the potential errors in physical dimensions must be calculated. Where repeated measurements were made at AEDC, error is taken as the standard deviation. When only one measurement was made, or the dimension was taken from another source, the magnitude of potential error was taken as plus or minus one-half of the least significant digit.

Calculation of Experimental Error

Signal

Voltages are measured by the EG&G 5206 lock-in amplifier. Device uncertainty = 0.1358 mV. All samples are 500 points.

E_S = bolometer signal response to source (80 to 290 mV),

E_T = bolometer signal response to chopper tare (7 to 40 mV),

E_{IC} = bolometer signal response to Internal Calibrator (41.3 mV).

Table C-1. Fluke 2204A Voltmeter Calibration (I-66727)

Input* (mV)	Voltage	No. of Readings	n	Mean ($\bar{x}$)	Bias (b)	Standard Deviation (σ)	Uncertainty (U)
0	0.017	13					
	0.018	20					
	0.019	6					
			39	0.01782051	0.01782051	0.00068333	0.01921587
1	1.017	4					
	1.018	35					
			39	1.01789744	0.01789744	0.00030735	0.01789744
5	5.015	1					
	5.016	28					
	5.017	1					
			30	5.016	0.016	0.00000007	0.01600014
10	10.015	3					
	10.016	24					
	10.017	3					
			30	10.016	0.016	0.00000021	0.01600042
20	20.018	16					
	20.019	12					
	20.020	2					
			30	20.01853333	0.01853333	0.00000040	0.01853414
50	50.010	3					
	50.011	25					
	50.012	2					
			30	50.01096667	0.01096667	0.00000017	0.01096702

Table C-1. (continued)

Input* (mV)	Voltage	No. of Readings	n	Mean ($\bar{x}$)	Bias (b)	Standard Deviation (σ)	Uncertainty (U)
100	100.036	4					
	100.037	20					
	100.038	6					
			30	100.0370667	0.0370667	0.00000034	0.03706739
150	150.029	2					
	150.030	28					
			30	150.0299333	0.0299333	0.00000006	0.02993342
200	200.008	27					
	200.009	3					
			30	200.0081	0.0081	0.00000019	0.00810038
250	250.000	16					
	250.001	13					
	250.002	1					
			30	250.0005	0.0005	0.00000033	0.00050066
300	300.026	24					
	300.027	6					
			30	300.0262	0.0262	0.00000017	0.02620034
Final			120		0.018080457	0.000111188	0.018300610

*Input from Analogic Voltage Standard (I-58381); calibration good through November 1984.

Table C-2. EG&G 5206 Lock-In Calibration (I-66950)

Input* (mV)	EG&G Reading	No. of Occur-rences	n	Mean ($\bar{x}$)	Bias (b)	Standard Deviation (σ)	Uncertainty (U)
5.0	4.98	1					
	4.99	9					
	5.0	30					
			40	4.99725	0.00275	0.00554122	0.01406517
10.0	9.97	1					
	9.98	3					
	9.99	6					
	10.0	13					
	10.01	5					
	10.02	2					
			30	9.998	0.002	0.0115669	0.02561961
20.0	19.97	1					
	19.98	3					
	19.99	11					
	20.0	8					
	20.1	5					
	20.2	2					
			30	19.9963333	0.0036667	0.01188547	0.279368
50.0	49.7	2					
	49.8	8					
	49.9	12					
	50.0	4					
	50.1	3					
	50.2	1					
			30	49.903333	0.0966667	0.11885469	0.33936794

Table C-2. (continued)

Input* (mV)	EG&G Reading	No. of Occur-rences	n	Mean ($\bar{x}$)	Bias (b)	Standard Deviation (σ)	Uncertainty (U)
100.0	99.8	1					
	99.5	5					
	100.0	10					
	100.1	8					
	100.2	7					
	100.3	2					
			33	100.0636364	-0.0636364	0.12454463	0.31795653
Final			163		0.032392646	0.052765849	0.135813568

*Input from PAR-124 lock-in calibrated output.

Table C-3 shows the voltage values obtained for bolometer signal.

Table C-3. Potential Voltage Error

	Minimum	Nominal	Maximum
E_S	289.8642	290	290.1358
E_T	9.8642	10	10.1358
E_b	299.7284	300	300.2716
E_{IC}	41.4358	41.3	40.86418

Source Temperature

Source temperature is computed from four voltage readings made by the Fluke 2204A voltmeter. The data range is from 1.99 to 220 mV, which corresponds to temperature variation from 391 to 283K. The device sensitivity is .05 mV per Kelvin in the upper range, and 5.28 mV per Kelvin in the lower range, with an uncertainty of 0.0183 mV. Temperature uncertainty is thus calculated as follows:

At a source temperature of 390.88K (1.99mV):

$$(\pm 0.0183 \text{ mV}) \times \left(\frac{1K}{0.05 \text{ mV}}\right) = \pm 0.366K$$

T =

Minimum	Nominal	Maximum
390.514	390.880	391.246

At a source temperature of 283K (111.74 mV):

$$(\pm 0.0183 \text{ mV}) \times \left(\frac{1K}{5.28 \text{ mV}}\right) = \pm 0.003466K$$

T =

Minimum	Nominal	Maximum
282.9965	283.0	283.0035

Bolometer Pinhole Diameter

0.125 cm nominal spec from IR Labs,

U = $\pm$0.0005 .

Detector-Source Separation

Detector-source separation is the sum of three measurements:

1. Bolometer inside distance, four measurements, no variation:

   3.769 in. $\pm$0.0005 in.

2. Bolometer to fixture distance, seven measurements:

   5.1955, 5.1905, 5.2029, 5.1930, 5.1975, 5.1908, 5.2012.

   a. Mean = 5.1969

   b. Average deviation from mean = $\pm$0.0062 in.

3. Fixture to source pinhole, two measurements:

   1.477 in. $\pm$0.01 in.

Total separation distance:

$$= 10.4419 \text{ in.} \pm 0.0167 \text{ in.}$$

$$= 26.5224 \text{ cm} \pm 0.0424 \text{ cm}$$

Calculation of Uncertainty

To obtain the experimental uncertainty, one must take the derivative of Eq. (C-4) with respect to each variable and then substitute the appropriate error value from above. Experimental uncertainty is summarized in Table C-4. Note that source area uncertainty has been ignored. Exclusion is justified because it has already been included in the source calibration uncertainty of 5 percent.

Table C-4. Derivation of Experimental Uncertainty

Uncertainty Derivation	Uncertainty at 390K (%)	Uncertainty at 283K (%)
$\frac{d(R_b)}{d\,r_b} \Big/ R_b = \frac{2\Delta r_b}{r_b} = \frac{\pm 2(0.0005)}{0.125} \times 100 =$	± 0.80	N/A
$\frac{d(R_b)}{dT} \Big/ R_b = \frac{4\ \Delta T}{T} = \frac{\pm 4(0.366)}{391} \times 100 =$	± 0.37	± 0.0049
$\frac{d(R_b)}{dE_{IC}} \Big/ R_b = \frac{\Delta E_{IC}}{E_{IC}} = \frac{\pm 0.1358}{41.3} \times 100 =$	± 0.33	N/A
$\frac{d(R_b)}{dD} \Big/ R_b = \frac{2\Delta D}{D} = \frac{\pm 2(0.0424)}{26.5224} \times 100 =$	± 0.32	N/A
$\frac{d(R_b)}{dE_b} \Big/ R_b = \frac{\Delta E_s}{} = \frac{\pm 0.2712}{E_b} \times 100 =$	± 0.09	± 0.27
Experimental Uncertainty	± 1.91	± 1.725

VITA

Kenneth A. Lienemann is employed as a project engineer for Calspan Corporation at Arnold Engineering Development Center (AEDC), Arnold Air Force Station, Tennessee. He had previously worked for Goodyear Tire and Rubber Company as a Programmer/Analyst. Mr. Lienemann attended high school in Papillon, Nebraska, and received a Bachelor of Science degree in Mechanical Engineering from the University of Nebraska. While involved in sensor testing technology at AEDC, he has developed a strong interest in Remote Sensing/Resource Management.
Mr. Lienemann attended The University of Tennessee Space Institute on a part-time basis, and in June 1985 he was awarded the Master of Science degree in Engineering Science.